การเปลี่ยนโครงสร้างเชิงวัฏภาคและสมบัติของสารประกอบ $ZnO_{1-x}S_x$ และ $ZnO_{1-x}Se_x$ ภายใต้สภาวะรุนแรง

นายรัฐ มโนธัม

วิทยานิพนธ์นี้เป็นส่วนหนึ่งของการศึกษาตามหลักสูตรปริญญาวิทยาศาสตรดุษฎีบัณฑิต
สาขาวิชาฟิสิกส์ ภาควิชาฟิสิกส์
คณะวิทยาศาสตร์ จุฬาลงกรณ์มหาวิทยาลัย
ปีการศึกษา 2558

STRUCTURAL PHASE TRANSITIONS AND PROPERTIES OF $ZnO_{1-x}S_x$ AND $ZnO_{1-x}Se_x$ UNDER EXTREAME CONDITIONS

Mr. Rut Manotum

A Dissertation Submitted in Partial Fulfillment of the Requirements
for the Degree of Doctor of Philosophy Program in Physics
Department of Physics
Faculty of Science
Chulalongkorn University
Academic Year 2015

Thesis Title	STRUCTURAL PHASE TRANSITIONS AND PROPERTIES OF $ZnO_{1-x}S_x$ AND $ZnO_{1-x}Se_x$ UNDER EXTREAME CONDITIONS
By	Mr. Rut Manotum
Field of Study	Physics
Thesis Advisor	Assistant Professor Thiti Bovornratanaraks, Ph.D.

Accepted by the Faculty of Science, Chulalongkorn University in Partial Fulfillment of the Requirements for the Doctoral Degree

.....Dean of the Faculty of Science
(Associate Professor Polkit Sangvanich, Ph.D.)

THESIS COMMITTEE

.....Chairman
(Assistant Professor Patcha Chatraphorn, Ph.D.)
.....Thesis Advisor
(Assistant Professor Thiti Bovornratanaraks, Ph.D.)
.....Examiner
(Assistant Professor Sakuntam Sanorpim, Ph.D.)
.....Examiner
(Assistant Professor Auttakit Chatrabhuti, Ph.D.)
.....External Examiner
(Associate Professor Anucha Yangthaisong, Ph.D.)

รัฐ มโนธัม : การเปลี่ยนโครงสร้างเชิงวัฏภาคและสมบัติของสารประกอบ $ZnO_{1-x}S_x$ และ $ZnO_{1-x}Se_x$ ภายใต้สภาวะรุนแรง (STRUCTURAL PHASE TRANSITIONS AND PROPERTIES OF $ZnO_{1-x}S_x$ AND $ZnO_{1-x}Se_x$ UNDER EXTREAME CONDITIONS) อ.ที่ปรึกษาวิทยานิพนธ์หลัก: ผศ. ดร. ธิติ บวรรัตนารักษ์, หน้า.

วิทยานิพนธ์นี้ได้ศึกษาการเปลี่ยนแปลงโครงสร้างและความเสถียรภายใต้ภาวะความดันสูงของ $ZnO_{0.5}S_{0.5}$, $ZnO_{0.5}Se_{0.5}$ และ $Zn_{16}O_1S_{15}$ ด้วยวิธีฟังก์ชันนัลของความหนาแน่น งานก่อนหน้านี้ได้เสนอโครงสร้างที่เป็นไปได้สำหรับ $ZnO_{0.5}S_{0.5}$ และ $ZnO_{0.5}Se_{0.5}$ ไว้ทั้งหมด 5 โครงสร้างกล่าวคือ Chalcopyrite, Rocksalt, Zincblende, Wurtzite และ CuAu-I ซึ่งโครงสร้างทั้งหมดได้ถูกศึกษาเพื่อหาโครงสร้างที่มีเสถียรภาพอย่างแท้จริง ทั้งในภาวะความดันบรรยากาศปกติ รวมทั้งขยายผลไปถึงความเสถียรของโครงสร้างและสมบัติต่างๆภายใต้ภาวะความดันสูง ด้วยวิธีการหลากหลายวิธี ซึ่งในงานวิจัยนี้ได้ศึกษาสมบัติของ $ZnO_{0.5}S_{0.5}$และ $ZnO_{0.5}Se_{0.5}$ ไปถึงความดัน 30 GPa จากผลการวิจัยชิ้นนี้สามารถยืนยันได้ว่า โครงสร้าง Chalcopyrite เป็นโครงสร้างที่เสถียรได้จนถึงความดัน 10 GPa ในขณะที่โครงสร้าง CuAu-I ซึ่งมีผู้เสนอไว้เช่นเดียวกันนั้นสามารถยืนยันได้จากงานวิจัยนี้ว่าไม่มีความเสถียร ซึ่งสามารถอธิบายได้ถึงโครงสร้างที่สามารถเกิดขึ้นได้ของ $ZnO_{0.5}S_{0.5}$ และ $ZnO_{0.5}Se_{0.5}$ ในภาวะ0-10 GPa สำหรับในกรณีของ $Zn_{16}O_1S_{15}$ นั้น ได้มีผู้เสนอโครงสร้างซึ่งได้จากการสังเคราะห์ด้วยวิธีการที่ต่างกันทั้งสิ้น 2 โครงสร้าง คือ Wurtzite และ Zincblende ในงานวิจัยชิ้นนี้ได้ศึกษาศึกสมบัติของโครงสร้างที่เป็นไปได้ทั้ง 2 แบบ รวมทั้งศึกษาสมบัติและความเสถียรของโครงสร้างไปถึงช่วงความดัน 20 GPa จากผลการศึกษาความเสถียรด้วยการคำนวณพบว่า สำหรับโครงสร้าง Zincblende นั้นสามารถเสถียรได้ถึงความดัน 10 GPa ซึ่งต่างจากโครงสร้าง Wurtzite ที่มีความเสถียรได้จนถึงความดัน 20 GPa ทั้งนี้ผู้วิจัยยังได้ศึกษาสมบัติทางไฟฟ้าของโครงสร้างที่เสถียรดังกล่าวภายใต้ความดัน เพื่อความเป็นไปได้ในการปรับใช้กับการปรับแต่ช่องว่างพลังงานด้วยความดันอีกด้วย

ภาควิชา ฟิสิกส์ ลายมือชื่อนิสิต .....

สาขาวิชา ฟิสิกส์ ลายมือชื่อ อ.ที่ปรึกษาหลัก .....

ปีการศึกษา 2558

5373821623 : MAJOR PHYSICS
KEYWORDS: PHASE STABILITY, ELASTIC PROPERTIES, HIGH PRESSURE, II-VI TERNARY ALLOYS

RUT MANOTUM: STRUCTURAL PHASE TRANSITIONS AND PROPERTIES OF $ZnO_{1-x}S_x$ AND $ZnO_{1-x}Se_x$ UNDER EXTREAME CONDITIONS. ADVISOR: ASST. PROF. THITI BOVORNRATANARAKS, Ph.D., pp.

Structures and high pressure phase transitions in $ZnO_{0.5}S_{0.5}$, $ZnO_{0.5}Se_{0.5}$ and $Zn_{16}O_1S_{15}$ have been investigated using density functional theory calculation. The previously proposed structures of $ZnO_{0.5}S_{0.5}$ and $ZnO_{0.5}Se_{0.5}$ which are Chalcopyrite, Rocksalt, Zincblende, Wurtzite and CuAu-I have been fully investigate Stability of these materials has been systematically studies up to 30 GPa for $ZnO_{0.5}S_{0.5}$ and $ZnO_{0.5}Se_{0.5}$ using various approached. In this thesis, we have confirmed the stability of Chalcopyrite structure up to at least 10 GPa where CuAu-I structure have been previously proposed. However, our calculation revealed that the CuAu-I is not a stable structure under this conditions which could explain the failure in several attempts to fabricate this materials under such conditions. We have also examined the pressure dependence of the bandgap and electronic structure up to 30 GPa. For $Zn_{16}O_1S_{15}$, two candidate structures namely Wurtzite and Zincblende were examined theirs properties and structures stability up to 20 GPa. The two exists phase which occurred during the difference film growth conditions was explained. Phonon dispersion and the Born criteria reveal that Zincblende is only be stable up to 10 GPa. Besides, Wurtzite structure yield no imaginary phonon frequencies and also satisfy the elastic constants sufficiency condition up to 20 GPa. The electronic structure and PDOS were fully investigated using HSE06. The electronic structure calculation provided mid O-3 state between fundamental ZnS band gap. The pressure effect on their electronic structure has been investigated for possibly adjustable optoelectronic device.

Department: Physics Student's Signature .....
Field of Study: Physics Advisor's Signature .....
Academic Year: 2015

ACKNOWLEDGEMENTS

I am very grateful to my supervisor, Asst. Prof. Dr. Thiti Bovornratanaraks, and Assoc. Prof. Dr. Udomsilp Pinsook who always advise and push me to pass through struggling PhD thesis. Thank you to big warm love from my family and my girlfriend who always beside when I feel down during PhD study . Thank you to ECPRL memberships, Dr. Rakchat Klinkla, Dr. Komsilp Kotmool, Prutthipong Tsuppayakorn-aek, Teerachote Pakornchote and Sorajit Areerat who help me a lot.

CONTENTS

Page

LIST OF TABLES

LIST OF FIGURES

Chapter 1
INTRODUCTION

Recently, the solar cell efficiency competitive has drawn significant interest from scientist of various disciplines since the energy crisis is one of the world's major problems. The doping II-VI semiconductors, such as in ZnO and ZnS, are promising candidate for blue range optoelectronic and spintronic devices. Besides, the $ZnO_{1-x}S_x$ and $ZnO_{1-x}Se_x$ ternary alloys have been synthesized for electronic and optical devices with the wide range of applications as well. In the band gap-engineering point of view, doping cation or anion in both II-VI and III-V lead to a large reduction in band gap. The Band-anticrossing (BAC) model was used to describe electronic band structure of mismatched alloys. From the BAC, the anticrossing interaction between N localized states and conduction band states in a host semiconductor causes the band gap bowling effect [1, 2]. The lager bowling parameters of ZnOS and ZnOSe than those of GaNP and GaNAs were expected that it is due to large differences in electronegativity of O, S and Se [3]. Due to large bowing parameter, II-VI semiconductor would be substitute for more adjustable solar cell device, which early has been dominated by III-V group. Lehr et al. [4] reported that using special molecular precursors, they can adjust the concentration of S in $ZnO1\text{-}_xS_x$, whereas the latter is adjusted via special organometallic precursor molecule for more suitable for light absorption in any range. In 2004, Meyer et al. [5] report that using radio-frequency reactive sputtering, a series of $ZnO_{1-x}S_x$ films with $0 \leq x \leq 1$ was deposited on different substrate. The x-ray diffraction (XRD) measurements were used to reveal the structure. The researchers found that the films have Wurtzite symmetry. The fundamental energy gaps of $ZnO_{1-x}S_x$ films were shown in Fig. 1. Even through, the films were growth in most composition but the structure and electronic property of $ZnO_{0.5}S_{0.5}$ (x = 0.5) are still in doubt due to solubility limit and substitutionally random alloys.

Rozale et al. [6] reported the structure and properties of ordered $ZnO_{1-x}S_x$ alloys calculation in various structure (CuAU-I, Cu_3Au, Luzonite and Famatinite) using local-density approximation (LDA) and Landau-Lifshitz theory of order-disorder transformation. The calculations result yield that Chalcopyrite and CuAu-I

were only two candidate structures of $ZnO_{0.5}S_{0.5}$ at 0 GPa. However, the electronic properties calculation result was underestimate compare with the experimental result due to LDA exchange correlation functional. According to Fan et al. [7], in order to include the random anion site of alloy, special quasi-random structure (SQSs) with LDA was used to investigate the structure and properties of $ZnO_{1-x}S_x$. Wurtzite supercells ($2 \times 1 \times 2, 2 \times 2 \times 1$) and Zincblende ($1 \times 1 \times 2$) structure were treated as model structure. The result yield that the lowest enthalpy structure of $ZnO_{0.5}S_{0.5}$ at 0 GPa is Chalcopyrite structure.

Thangavel et al. [8] computed the electronic properties and total energy of five different structures of $ZnO_{0.5}S_{0.5}$ and $ZnO_{0.5}Se_{0.5}$ namely Chalcopyrite, Wurtzite, Zincblende, CuAu-I and Rocksalt using LDA as exchange correlation function. The initial lattice parameters of all structures were obtain by Vegard's law, which is $a(A_{1-x}B_xC)_{alloy} = (1-x)a_{AC} + xa_{BC,}$ where AC stand for ZnO and BC stand for ZnS or ZnSe. By comparing the total energy with decreasing volume (E-V curve), the result yield that the lowest total energy at 0 GPa of both ternary alloys were Chalcopyrite structure. Khan and Ahmad [9] investigated the electronic band structure and partial density of state (PDOS) of $ZnO_{1-x}S_x$ using modified Becke and Johnson (mBJ) exchange potential comparing with LDA, GGA and corrected LDA in all compositions on Zincblende structure. The results yield that both LDA and GGA significantly underestimate the band gap from experimental values. The correct LDA yield non-reliable results but the mBJ potential calculation results are very close to the experimental results, with less than 2% error.

Although, the previous researchers performed computational work on the structure and properties of $ZnO_{0.5}S_{0.5}$ and $ZnO_{0.5}Se_{0.5}$ at 0 GPa, there were such theoretical reports, it is still unclear that which structure is stable at ambient condition owing to insufficient dynamical information of the system, e.g. phonon dispersion and structural dynamics at nonzero temperature.

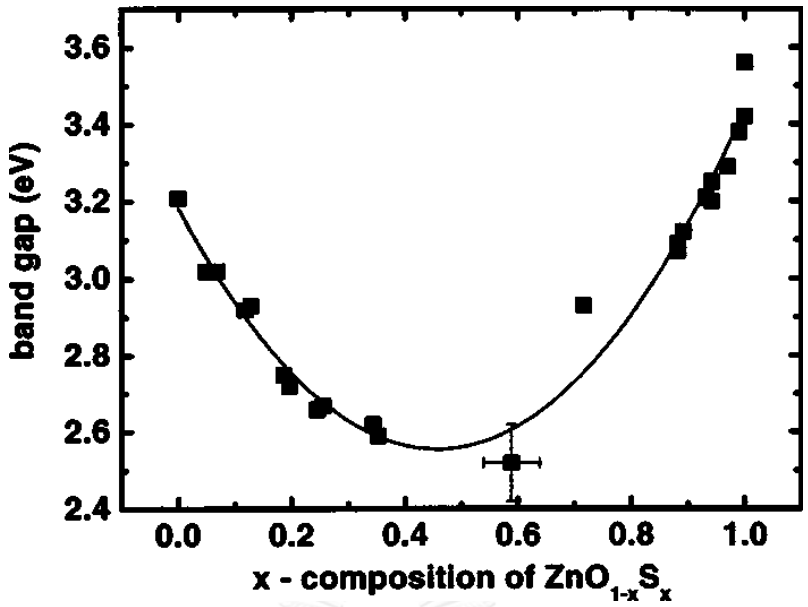

Figure 1: Band gap energy of $ZnO_{1-x}S_x$ as a function of composition x [5].

Not only the ternary alloy is interested among the researchers but also II-VI doped semiconductor. A lot of theoretical and experimental works have been done on doping II-VI system. Pan et al. [10] reported that a series of $ZnO_{1-x}S_x$ ($0 \leq x \leq 1$) were grown on quartz substrates by radio-frequency (rf) magnetron sputtering of ZnS ceramic target, using oxygen and argon as working gas. The films were grown for 2 h at substrates temperature of 573K and were annealed in temperature range 773-873 K. XRD with Cu K_α radiation was used to characterize the structure of the film. X-ray photoelectron spectroscopy (XPS) were used to analyze the composition of the films. The structures in O-rich side $0 < x < 0.23$ were Wurtzite and S-rich side ($0.77 \leq x \leq 1$) were Zincblende structure. However, the films were consistent of 2 phases or amorphous in the range of $0.23 < x < 0.77$. On the other hand, He et al. [11] reported interesting different result. The researchers synthesized $ZnO_{1-x}S_x$ thin film on sapphire substrates by pulse laser deposition. A ZnS ceramic was used as target with varying oxygen partial pressure in order to adjust O composition. The substrate temperature was kept constant at 750 °C while the O_2 partial pressure was varied in the range 0-6 GPa. XRD using both a power diffractometer and a four-circle single crystal diffractometer were performed for structural characterization. XPS was used to

analyze the composition of $ZnO_{1-x}S_x$ films. Wurtzite structures were observed in composition range of $0 \leq x \leq 0.23$ and $0.94 \leq x \leq 1$. All of the others compositions $(0.23 < x < 0.94)$ were phase separation of ZnO and ZnS. Even the researcher reported different structure in doping ZnS by O $(0.94 \leq x \leq 1)$ but the theoretical conditions are still in doubt; furthermore, no calculation work on their properties and stability under high pressure has been done yet.

Elastic properties of solid are important due to fundamental solid-state phenomena such as equation of state, phonon spectra and atomic potentials. Furthermore, the elastic stiffness coefficients are essential for many applications to mechanical properties of solid such as internal strain and thermoelastic stress. However, only a few studies have conduct on the mechanical properties of $ZnO_{0.5}S_{0.5}$, $ZnO_{0.5}Se_{0.5}$ and O doped in ZnS at high pressure condition. Bilge et al. [12] reported that ZnS crystallizes in cubic Zincblende and Wurtzite structure at ambient pressure condition. There is a phase transition from Wurtzite to Zincblende and from Zincblende to Rocksalt when the pressure is applied. For O doped in ZnS, the high-pressure phase hasn't been revealed yet.

Yu et al. [13] investigated multiple electronic band gap semiconductors in $Zn_{1-y}Mn_yO_xTe_{1-x}$. Those alloys have been synthesized using the combination of oxygen ion implantation and pulse laser melting. Only 1.3% O doped that substituted Te atom in a $Zn_{0.88}Mn_{0.12}Te$ host lead to the formation of a narrow, oxygen-derived band of extend state locate within the band gap of host. The researchers demonstrate that these type of alloys fulfill the criteria for three-band semiconductor that has been propose of making high efficiency, single-junction solar cells. Ishikawa and Nakayama [14] performed first principle calculation to investigate the electronic structure on O doped in II-VI (ZnS, ZnSe and ZnTe) semiconductor using GGA as exchange correlation energy. The $2 \times 2 \times 2$ Zincblende supercells that contain 32 Zn and 32 atom of VI (S, Se and Te) were created as a host. To simulate O doping in the II-VI semiconductor, one of the VI atom were substituted with O, which correspond to the 3% doping comparable to experimental. The result yield that a narrow O originate state occurred in host ZnTe band gap as expected; on the other hand, the doped O state was

interpreted to be hybridization state of O with conduction band state of host in ZnS and ZnSe. The electronic structure of ZnS. ZnSe and ZnTe were shown in Fig. 2.

According to previous works, the knowledge about the structure and properties of $ZnO_{0.5}S_{0.5}$, $ZnO_{0.5}Se_{0.5}$ and O doped in ZnS under pressure should be investigated; especially, the structure stability and electronic structure due to opportunity to become a promising optoelectronic device. In this thesis, we simulated the structure of $ZnO_{0.5}S_{0.5}$, $ZnO_{0.5}Se_{0.5}$ and $Zn_{16}O_1S_{15}$ using Cambridge Serial Total Energy Package (CASTEP) code base on density functional theory (DFT) with GGA and Heyd-Scuseria-Ernzerhof (HSE). The mechanical, electronic properties and corresponding stability under pressure of $ZnO_{0.5}S_{0.5}$, $ZnO_{0.5}Se_{0.5}$ up to 30 GPa and $Zn_{16}O_1S_{15}$ up to 20 GPa were investigated. The geometry optimizations have been done for all structures. The electronic structure, PDOS and elastic stiffness constants are reported the first time in this work.

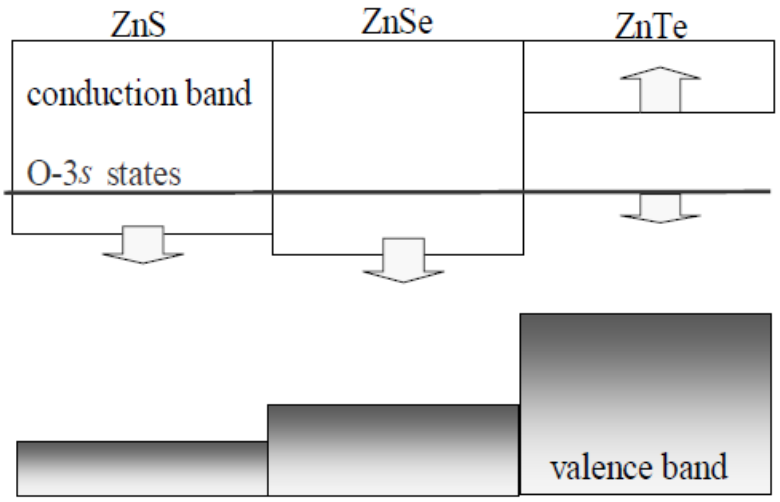

Figure 2: Schematic illustration of energy position of O-originate states in ZnS, ZnSe and ZnTe [14].

The organization of the thesis is as follows: In Chapter 2 we describe the theory is used in this work. Chapter 3 contains the results for structure stability such as enthalpy, phonon dispersion and elastic stiffness constant. Chapter 4 gives the information about electronic structure and also PDOS of the stable structure. The conclusions of this work were presented in Chapter 5.

Chapter 2
THEORETICAL BACKGROUND

2.1 Many body problem

Solid is composed of many electrons and nucleus which interaction to one another. Therefore, the many body problem needs to be solved inevitably. In classical mechanics, the solution for more than 3 particles interaction problem cannot be solved exactly. The study of electron and nucleus, therefore, needs the quantum mechanics to find the accurate answers.

To solve this problem, for quantum mechanics, we apply Schrodinger equation as follows;

$$\hat{H}\Psi = E\Psi\,, \tag{2.1}$$

where E is energy of the solid system, ψ is the wavefunction and $\hat{H}$ is the Hamiltonian operator. Hamiltonian operator in solid (system) consists of electron and nucleus, as follows;

$$\hat{H} = \hat{T}_e + \hat{V}_{e-e} + \hat{V}_{n-e} + \hat{T}_n + \hat{V}_{n-n}\,, \tag{2.2}$$

The terms are kinetic energy of electron, Coulomb potential energy between electrons, kinetic energy of nucleus, and potential energy between nucleuses respectively. The exact Hamiltonian in Eq. (2.2) is in differential form. One of the most powerful tools to obtain the solution is the separation variable method. However, this method cannot be used due to the Coulomb potential cannot decouple.

In order to simplify this problem, Born and Oppenheimmer proposed that in the adiabatic condition, the wave functions of electron and nucleus are separable function. Thus, the Schrodinger equation for electron and nucleus can be solved separately which we focus on electron. Because most of solid's properties are depended on electron. Eq. (2.2) reduced to

$$\hat{H} = \hat{T}_e + \hat{V}_{e-e} + \hat{V}_{n-e}\,. \tag{2.3}$$

Even though the wave function of electron and nucleus are separable but the Coulomb potential between electron and electron, as show in the second term in Eq. (2.3), are coupling. In order to solve this problem, Hartree used the orthogonal electron's wave function which is,

$$\Psi_H = \varphi(\boldsymbol{r}_1)\varphi(\boldsymbol{r}_2)...\varphi(\mathrm{r}_n), \tag{2.4}$$

as the solution of Eq. (2.3). However, the Hartree energy, defined as E_H, is higher than the ground state energy in well-known system. In order to improve the Hartee approximation, Hartee and Fock added the electron's behavior. Due to electron is indistinct particle and must obey the Puali exclusion principle, lead to the anti-symmetric electron wave function. The improved solution was represented in Slater determinant form as follow;

$$\Psi_{HF} = \frac{1}{\sqrt{N!}}\det\left[\varphi_1\varphi_2...\varphi_n\right]. \tag{2.5}$$

The anti-symmetric wave function provide lower energy, namely Hartre-Fock energy E_{HF}, than Hartee energy. However, E_{HF} is still higher than the ground state energy due to correlation energy. Fig. 3 show the energy level of E, E_x and E_c. The exchange energy was defined by

$$E_x = E_H - E_{HF}\ , \tag{2.6}$$

and the correlation energy was defined by

$$E_c = E_{HF} - E\ . \tag{2.7}$$

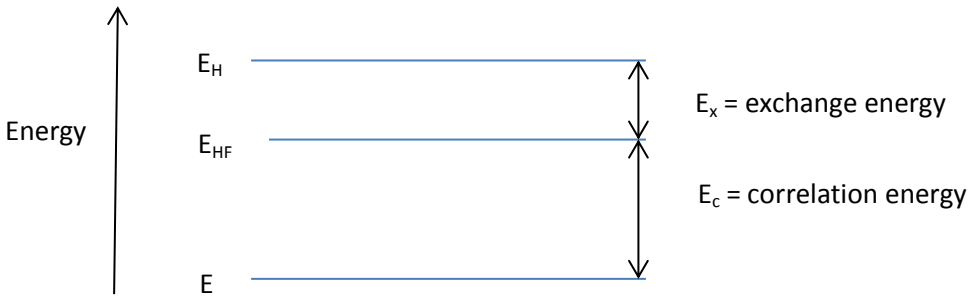

Figure 3: The ground state energy level calculated by Hatree and Hartree-Fock approximation.

2.2 Density function theory

In order to investigate the ground state of many body systems, the density function theory is the other way to solve Eq. (2.3). This method simplifies the n-body equation to the n equation of one body. Density function theory (DFT) has been used due to low computational cost requirement and flexibility, nowadays even the personal computer (PC) can perform the DFT calculation.

In DFT, the energy of the system was represented by the functional of density of electron as follow;

$$E[\rho] = \mathrm{T}[\rho] + \mathrm{V}_{e-e}[\rho] + \mathrm{V}_{ext}[\rho] + \mathrm{V}_{xc}[\rho]. \tag{2.8}$$

The first term, T[ρ], represented the kinetic energy of non-interacting electron. The next term, $V_{e\text{-}e}[\rho]$, is the Coulomb potential between electron and electron. The third term, $V_{ext}[\rho]$, is called the external potential which is the Coulomb potential between electron and nucleus. The last term, $V_{xc}[\rho]$, is the exchange-correlation potential. The total number of electron (N) in many body system are defined by

$$N = \int \rho(\boldsymbol{r}) dV . \tag{2.9}$$

Two important theorems in the DFT were stated by Hohenbreng-Kohn. First, the external potential is unique for the corresponding electronic density, beside an additive constant. This first theorem is also easily described; the external potential is one on one mapping function with electron density. In order to demonstrate, we rewrite the Hamiltonian in term of electron density functional as density matrices as follows;

$$E[\rho] = T[\rho] + V_{ext}[\rho] + U[\rho], \tag{2.10}$$

where

$$T(\rho) = \int -\frac{1}{2} \nabla_r^2 \rho_1(\boldsymbol{r}', \boldsymbol{r})_{\boldsymbol{r}'=\boldsymbol{r}} d\boldsymbol{r}, \tag{2.11}$$

$$V_{ext}(\rho) = \int v(\boldsymbol{r}) \rho(\boldsymbol{r}) d\boldsymbol{r}, \tag{2.12}$$

$$U(\rho)=\iint \frac{1}{\boldsymbol{r}_1-\boldsymbol{r}_2}\rho_2\left(\boldsymbol{r}_1^{'}\boldsymbol{r}_2^{'},\boldsymbol{r}_1\,\boldsymbol{r}_2\right)\boldsymbol{d}\boldsymbol{r}_1\,d\boldsymbol{r}_2\ , \tag{2.13}$$

where $\rho_N\left(\boldsymbol{r}_1^{'}\boldsymbol{r}_2^{'}\cdots\boldsymbol{r}_N^{'},\boldsymbol{r}_1\boldsymbol{r}_2\cdots\boldsymbol{r}_N\right)$ is the N particle density matrices defined by

$$\rho_N(\boldsymbol{r}_1^{'}\boldsymbol{r}_2^{'}\cdots\boldsymbol{r}_N^{'},\boldsymbol{r}_1\,\boldsymbol{r}_2\,\cdots\boldsymbol{r}_N)=\psi_N\left(\boldsymbol{r}_1^{'}\boldsymbol{r}_2^{'}\cdots\boldsymbol{r}_N^{'}\right)\psi_N^{*}\left(\boldsymbol{r}_1\,\boldsymbol{r}_2\,\cdots\boldsymbol{r}_N\right). \tag{2.14}$$

The first term in Eq. (2.10), $T[\rho]$, is non-interacting kinetic energy of electron. The second term, $V_{ext}[\rho]$, is the potential energy from nucleus of system and latter is the potential energy between electrons. We suppose that the external energy is not uniquely determined by electron density. We should be able to find two external potential V,V' corresponding to ground state energy with the same ρ. Let ϕ be the ground state of the Hamiltonian $\hat{H}=\hat{T}+\hat{V}_{ext}+\hat{U}_{ee}$ that provides the ground state energy $E_0=\left\langle\phi\middle|\hat{H}\middle|\phi\right\rangle$. Let ϕ' be the ground state of another Hamiltonian $\hat{H}'=\hat{T}+\hat{V}_{ext}^{'}+\hat{U}_{ee}$ which provides ground state energy $E_0^{'}=\left\langle\phi'\middle|\hat{H}^{'}\middle|\phi'\right\rangle$. We have

$$E_0<\left\langle\phi'\middle|\hat{H}\middle|\phi'\right\rangle=\left\langle\phi'\middle|\hat{H}^{'}\middle|\phi'\right\rangle+\left\langle\phi'\middle|\hat{H}-\hat{H}^{'}\middle|\phi'\right\rangle\ , \tag{2.15}$$

$$=E_0^{'}+\int\rho(\boldsymbol{r})\left[v_{ext}(\boldsymbol{r})-v_{ext}^{'}(\boldsymbol{r})\right]d\boldsymbol{r}\,, \tag{2.16}$$

and vice versa,

$$E_0^{'}<\left\langle\phi\middle|\hat{H}^{'}\middle|\phi\right\rangle=\left\langle\phi\middle|\hat{H}\middle|\phi\right\rangle+\left\langle\phi\middle|\hat{H}^{'}-\hat{H}\middle|\phi\right\rangle\ , \tag{2.17}$$

$$=E_0+\int\rho(\boldsymbol{r})\left[v_{ext}^{'}(\boldsymbol{r})-v_{ext}(\boldsymbol{r})\right]d\boldsymbol{r}\,. \tag{2.18}$$

Adding Eq. (2.16) and (2.18), we get

$$E_0+E_0^{'}<E_0+E_0^{'}, \tag{2.19}$$

which is not possible. Therefore, we can conclude that one electron density of the system does not provides two difference $V_{ext}(\boldsymbol{r})$. In addition, the ground state density and their corresponding $V_{ext}(\boldsymbol{r})$ are confidently obtained at this point. The second theorem is that there is the only one exact ground state density, $\rho_0(\boldsymbol{r})$, which

provide the ground state energy of the system, E_0. The non-ground states densities, $\tilde{\rho}(\boldsymbol{r})$, yield higher energy than the lowest one. The ground state energy is defined by

$$E_0 = E\left[\rho_0(\boldsymbol{r})\right] \leq E\left[\tilde{\rho}(\boldsymbol{r})\right]. \tag{2.20}$$

2.3 Kohn-Sham method

Although the classical electron-electron interaction was considered by Hartree (the so call Hartee term) that Hatree-Fock modified later by adding exchange energy but certain amount of energy (in Quantum point of view) in many body problem is displaced, namely the correlation energy. In order to deal with the correlation energy, the density matrices come forth to play the main role of this problem. The electron density of the system in N particles many body problem is shown in Eq. (2.14). However, it is too difficult to deal with so many variables, so we reduced it into one particle problem as,

$$\rho_1(\boldsymbol{r}_1', \boldsymbol{r}_1) = N \int \cdots \int \rho_N(\boldsymbol{r}_1' \boldsymbol{r}_2' \cdots \boldsymbol{r}_N', \boldsymbol{r}_1 \boldsymbol{r}_2 \cdots \boldsymbol{r}_N) d\boldsymbol{r}_2 \cdots d\boldsymbol{r}_N . \tag{2.21}$$

To handle the two-electron interaction (Coulomb potential), the density matrices should be written down in two-particle problem as,

$$\rho_2(\boldsymbol{r}_1', \boldsymbol{r}_2', \boldsymbol{r}_1, \boldsymbol{r}_2) = \frac{N(N-1)}{2} \int \cdots \int \rho_N(\boldsymbol{r}_1' \boldsymbol{r}_2' \cdots \boldsymbol{r}_N', \boldsymbol{r}_1 \boldsymbol{r}_2 \cdots \boldsymbol{r}_N) d\boldsymbol{r}_2 \cdots d\boldsymbol{r}_N . \tag{2.22}$$

The Hamiltonian can be written in term of the density functional as Eq. (2.10). Moreover, the Coulomb potential is less complicated when the density matrices is reduced to one particle density matrices as follow,

$$J[\rho] = \frac{1}{2} \int \frac{1}{r_{12}} \rho(\boldsymbol{r}_1) \rho(\boldsymbol{r}_2) d\boldsymbol{r}_1 d\boldsymbol{r}_2 . \tag{2.23}$$

The Hatree potential which considers only classical part of Coulomb potential was represented in Eq. (2.23). Beside, we reduced the density matrices of two particles as,

$$\rho_2(\boldsymbol{r}_1', \boldsymbol{r}_2', \boldsymbol{r}_1, \boldsymbol{r}_2) = \frac{1}{2}\left[\rho(\boldsymbol{r}_1)\rho(\boldsymbol{r}_2) + \rho(\boldsymbol{r}_1)\rho_{xc}(\boldsymbol{r}_1, \boldsymbol{r}_2)\right], \tag{2.24}$$

which is separated into classical and quantum part. The ρ_{xc} term is the exchange-correlation hole which provide the exchange-correlation energy,

$$E_{xc}[\rho] = \frac{1}{2}\iint \frac{1}{r_{12}} \rho(\boldsymbol{r}_1)\rho_{xc}(\boldsymbol{r}_1,\boldsymbol{r}_2)\,d\boldsymbol{r}_1 d\boldsymbol{r}_2 . \tag{2.25}$$

The energy functional in Eq. (2.10) becomes

$$E[\rho] = T[\rho] + J[\rho] + E_{xc}[\rho] + V_{ext}[\rho]. \tag{2.26}$$

Due to Kohenberg-Kohn second theorem, we performed the vibrational method to find the extremum path

$$\frac{\delta E[\rho]}{\delta \rho[\boldsymbol{r}]} = 0, \tag{2.27}$$

which lead to

$$\int \delta\rho(\boldsymbol{r}) \left\{ -\frac{1}{2}\nabla^2 + v_{eff}(\boldsymbol{r}) \right\} d\boldsymbol{r} = 0, \tag{2.28}$$

when $v_{eff}(\boldsymbol{r})$ is defined as

$$v_{eff}(\boldsymbol{r}) = \int \frac{\rho(\boldsymbol{r}')}{|\boldsymbol{r}-\boldsymbol{r}'|} d\boldsymbol{r}' + \boldsymbol{v}(\boldsymbol{r}) + \frac{\delta E_{xc}[\rho]}{\delta \rho[\boldsymbol{r}]}. \tag{2.29}$$

In this point of view, the non-interacting electrons are moving in the effective potential $v_{eff}(\boldsymbol{r})$**.** Due to the $\rho(\boldsymbol{r})$ is satisfied Eq. (2.27) condition, the solution of Eq. (2.28) and (2.29) are obtained by one-particle Schrödinger's equation in atomic unit

$$\left\{ -\frac{1}{2}\nabla^2 + v_{eff}(\boldsymbol{r}) \right\} \boldsymbol{\psi}_i^{KS}(\boldsymbol{r}) = \varepsilon_i \boldsymbol{\psi}_i^{KS}(\boldsymbol{r}), \tag{2.30}$$

when

$$\rho(\boldsymbol{r}) = \sum_{i=1}^{N} \left| \boldsymbol{\psi}_i^{KS}(\boldsymbol{r}) \right|^2 . \tag{2.31}$$

The $\psi_i^{KS}(\boldsymbol{r})$ is the Kohn-Sham orbital. The $\rho(\boldsymbol{r})$ can be solved self-consistently by Eq. (2.29)-(2.31) that is known as the Kohn-Sham method.

2.4 Exchange-correlation energy

The Kohn-Sham method is the powerful tool to obtain the accurate total energy of many electrons system. According to Eq. (2.7), the total energy of any solid system can be represented in term of electron's density functional. The first three term is well-known form but the exact form of the last, exchange-correlation energy, is still questionable functional. Therefore, the exact mapping between electron's density and total energy cannot be written in an explicit form.

The exchange-correlation energy can be separated into two term the exchange energy, $E_x[\rho]$, and correlation energy, $E_c[\rho]$, as

$$E_{xc}[\rho] = E_x[\rho] + E_c[\rho]. \tag{2.32}$$

The exchange energy, arises from an antisymmetric wavefunction was represented by Hatree-Fock approximation in the explicit form as

$$E_x^{exact}[\rho] = -\iint \varphi_j(\boldsymbol{r})\varphi_j^*(\boldsymbol{r}')\frac{1}{|\boldsymbol{r}-\boldsymbol{r}'|}\varphi_i(\boldsymbol{r})\varphi_i^*(\boldsymbol{r}')\,\mathrm{d}\boldsymbol{r}\,\mathrm{d}\boldsymbol{r}'. \tag{2.33}$$

However, this exact form is not widely used in the DFT calculation because it is non-local.

There are so many approaches that were proposed lately. They can be classified by approximate method as shown in Fig. 4. According to Fig. 4, the higher approach lead to more accurate result but it costs more resource. Thus, we have to optimize between the acceptable output and the resource. In this thesis we used two exchange-correlation functional, i.e. GGA and Hybrid GGA.

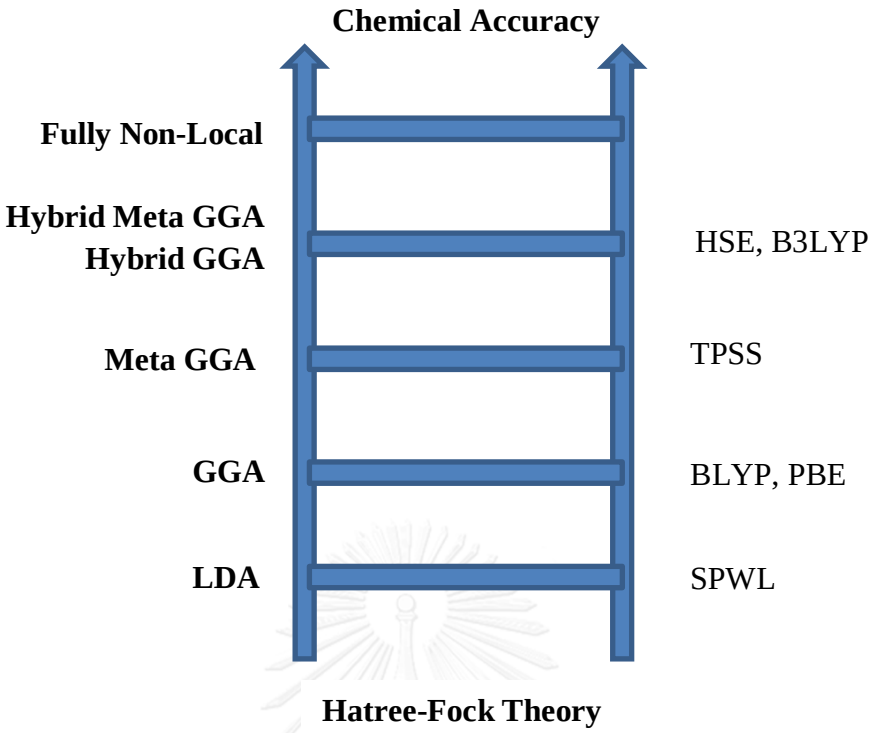

Figure 4: Jacob's ladder for the five generation of DFT functionals.

The first exchange-correlation that was chosen, GGA proposed by Perdew-Burke-Ernzerfof (PBE), which is not only consider the electron's density but to supplement the density with information about the gradient of the charge density, $\nabla\rho(\mathrm{r})$ in order to account for the non-homogeneity of the electron density as follows;

$$E_{xc}^{GGA}[\rho] = \int v_{xc}(\rho, |\nabla\rho|)\rho d\boldsymbol{r} \,. \tag{2.34}$$

Even though the GGA provided good result in atomic and molecular energy but their electronic structure results do not agree with experimental results. There are two reasons for this problem. First, the DFT method can only predict the ground state density. Second, this approach approximated that the exchange-correlation energy is the semi-local potential instead of non-local potential in real system. Therefore, the Hybrid approach is introduced.

To treat the non-local effect, the Hybrid included the Hartree-Fork exchange energy with the exchange-correlation function in DFT as

$$E_{xc}^{hyb} = \alpha E_x^{HF} + (1-\alpha) E_x^{DFT} + E_c^{DFT}, \quad (2.35)$$

where α is either chosen or is fit to some properties of a molecular data base. There are many Hybrid functionals have been proposed. In thesis, we used Heyd-Scuseria-Emzerhof (HSE) functional. In the HSE scheme, not only HF exchange energy is included but also the screened Coulomb potential is arise. The GGA-PBE exchange and correlation energy are chosen to represent E_x^{DFT} and E_c^{DFT}. In this functional the division of exchange interaction has been proposed in short-range (SR), $E_x^{PBE,SR}$, and long-range part (LR), $E_x^{PBE,LR}$, as shown

$$E_{xc}^{hyb} = \alpha E_x^{HF,SR}(\omega) + (1-\alpha) E_x^{PBE,SR}(\omega) + E_x^{PBE,LR}(\omega) + E_c^{PBE}(\omega). \quad (2.36)$$

The coefficient α which is set as $\alpha = 0.25$ and using $\omega = 0.15$, which is a numerical tests based a realistic value. HSE has been improved more efficient in predicting the energy gap compared to normal GGA.

2.5 Plane wave Basis set

It is keep in mind that the atom in solid state arrange orderly. In non-interacting system, the electrons are moving in the periodic potential from nucleus. Therefore, the potential has to follow the Bloch's theorem

$$U(\boldsymbol{r}) = U(\boldsymbol{r} + \mathbf{T}), \quad (2.37)$$

where $\mathbf{T}$ is a translation vector. The $U(\boldsymbol{r})$ satisfied the periodicity in solid by this condition. In order to follows the Bloch's theorem, the electron wave function is written as

$$\Psi(\mathbf{r} + \mathbf{R}) = e^{i\mathbf{k}\cdot\mathbf{R}}\Psi(\mathbf{r}). \quad (2.38)$$

Using the Fourier's transformation, the electron wave function can be expressed as

$$\Psi(\mathbf{r}) = \frac{1}{\Omega}\sum_{m}\Psi(\mathbf{k}+\mathbf{G}_m)e^{i(\mathbf{k}+\mathbf{G}_m)\cdot\mathbf{r}}, \tag{2.39}$$

where $\mathbf{G}$ denotes the reciprocal lattice vector and Ω is the volume of solid system. The plane wave basis suit very well in Eq. (2.37).

2.6 Pseudopotenital

In many body problem, the most precise method is all electron calculation (AE). However, AE is the most expensive approach to perform calculation. In order to optimize resource, the pseudopotential method was introduced to simplify computing problem. The AE wave function can be separated into two parts, divided by cutoff radius (r_c), the core and valence wave function as suggested by Herring [15], Phillips and Kleinman [16]. The core electron wave function oscillates lead to the expensive resource, it required so many number of plane wave basis to represent core electron wave function. On the other hand, the valence wave function is smooth which mainly represent the interaction to other atoms and distributes around the Fermi surface. To reduce the computational cost, the core wave function can be replaced by effective potential, or pseudopotential as shown in Fig. 5. The pseudo wave function can be written as

$$\left|\psi_{ps}\right\rangle = \left|\psi\right\rangle - \sum_{c}\left|\psi_c\right\rangle\left\langle\psi_c\,|\,\psi_{ps}\right\rangle, \tag{2.40}$$

where ψ_c is the wave function in core region, so the summation is summed over the core states and ψ is the AE wave function. Thus, the Schrödinger's equation that satisfies the pseudo wave function is

$$H\left|\psi\right\rangle = E\left|\psi\right\rangle, \tag{2.41}$$

$$H(\left|\psi_{ps}\right\rangle + \sum_{c}\left|\psi_c\right\rangle\left\langle\psi_c\,|\,\psi_{ps}\right\rangle) = \mathrm{E}(\left|\psi_{ps}\right\rangle + \sum_{c}\left|\psi_c\right\rangle\left\langle\psi_c\,|\,\psi_{ps}\right\rangle), \tag{2.42}$$

$$H\left|\psi_{ps}\right\rangle + \sum_{c}(\mathrm{E}_c - \mathrm{E})\left|\psi_c\right\rangle\left\langle\psi_c\,|\,\psi_{ps}\right\rangle = E\left|\psi_{ps}\right\rangle, \tag{2.43}$$

where $H = -\frac{1}{2}\nabla^2 + V(\boldsymbol{r})$ and E_c is the eigenenergy of the core state, so that

$$(-\frac{1}{2}\nabla^2 + \mathrm{U}_{ps})\left|\psi_{ps}\right\rangle = E\left|\psi_{ps}\right\rangle, \tag{2.44}$$

where $U_{ps} = V(\boldsymbol{r}) + \sum(E_c - E)\left|\psi_{ps}\right\rangle\left\langle\psi_{ps}\right|$ is the pseudopotential. To avoid the AE calculation, the energy of many body systems can be calculated using pseudo wave function and pseudopotential instead.

In order to generate an accurate pseudopotential, Hamann, Schlűter and Chiang [17] proposed the conditions to generate norm-conserving pseudopotential as follows:

1. The eigenvalues of the real and pseudo system, E and E', respectively, are equivalent

$$E = E'. \tag{2.45}$$

2. The wave function outside the core region of the real and pseudo system are equivalent

$$\psi(\boldsymbol{r}) = \psi_{ps}(\boldsymbol{r}) \text{ for } r \geq r_c. \tag{2.46}$$

3. The integrals from 0 to R, when $R > r_c$ of the real and pseudo charge densities are equivalent (norm-conserving)

$$\langle\psi\,|\,\psi\rangle_R = \langle\psi_{ps}\,|\,\psi_{ps}\rangle_R. \tag{2.47}$$

4. The first energy derivatives of the logarithmic derivatives of the real and pseudo wave function are equivalent for $r > r_c$.

However, Vanderbit proposed that the norm-conserving constraint can be reduced [18]. It is so-called ultrasoft pseudopotential.

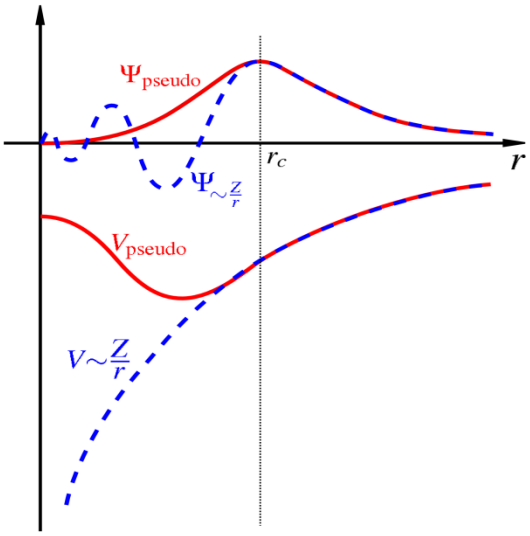

Figure 5: Comparison of a Coulomb potential and a compatible wavefunction of the nucleus (dash blue line) and of the pseudopotential (solid red line), wavefunctions and potentials of both are identical when above the cutoff radius, r_c.

2.7 Band structure

In order to construct the electronic band structure of solid system, Kohn-Sham has to be solved to obtain the ground state wave function and also corresponding Hamiltonian of the system. The information about properties of the solid system can be obtained by the 1st Brillouin zone. The energy level of the n^{th} band at wave vector k are obtained by

$$\left\langle \psi_{nk} \left| \hat{\mathrm{H}} \right| \psi_{nk} \right\rangle = E_{nk} . \tag{2.48}$$

This process yields the energy levels of any n band at various wave vector k, for constructing of band structure.

The density of states (DOS) for a given n^{th} band, $N_n(\mathrm{E})$, can be calculated from

$$N_n(\mathrm{E}) = \int \frac{dk}{4\pi^3} \delta(\mathrm{E} - \mathrm{E}_n(\mathrm{k})), \tag{2.49}$$

where $E_n(k)$ depicts the dispersion of the n^{th} band. The total density of state is obtained from the summation of all bands. In addition, the total number of electron in unit cell can be compute by the integral of DOS from the lowest energy to Fermi level.

2.8 Structure stability

2.8.1 Phonon calculation

The phonon calculation is performed to investigate the structure's stability under high pressure, the softening of phonon frequency in acoustic mode occur during the structure transformation. The imaginary value of phonon frequency implies that the crystal structure is in unstable phase.

The total energy expansion around the equilibrium point can be written as

$$E = E_0 + \sum_{\kappa,\alpha} \frac{\partial E}{\partial \mathbf{u}_{\kappa,\alpha}} \partial \mathbf{u}_{\kappa,\alpha} + \frac{1}{2} \sum_{\kappa,\alpha,\kappa',\alpha'} \mathbf{u}_{\kappa,\alpha} \cdot \Phi^{\kappa,\kappa'}_{\alpha,\alpha'} \cdot \mathbf{u}_{\kappa',\alpha'} + \ldots \qquad (2.50)$$

where $\mathbf{u}_{k,\alpha}$ is the atomic displacement from equilibrium position and $\Phi^{\kappa,\kappa'}_{\alpha,\alpha'}$ is the matrix of force constants $\Phi^{\kappa,\kappa'}_{\alpha,\alpha'} = \frac{\partial^2 E}{\partial \mathbf{u}_{k,\alpha} \partial \mathbf{u}_{k',\alpha'}}$. Due to the lowest energy at the equilibrium point, all of the others term except the first are the derivative of the energy with respect to $\mathbf{u}_{k,\alpha}$. Thus, the second term on the right hand side in Eq. 2.50, the 1^{st} order derivative is represented the force acting on the atom, are all zero. The fourth term and so on are assumed to be negligible. The third term represents the energy in harmonic approximation. The dynamical matrix is introduced, to obtain the phonon frequency, which is defined as

$$D^{\kappa,\kappa'}_{\alpha,\alpha'}(\mathbf{q}) = \frac{1}{\sqrt{M_\kappa M_{\kappa'}}} \Phi^{\kappa,\kappa'}_{\alpha,\alpha'}, \qquad (2.51)$$

where M_k is the mass of the nucleus. The solution of the Eq. (2.51) is obtained by eigenvalue equation,

$$D\varepsilon_m = \omega_m^2 \varepsilon_m . \qquad (2.52)$$

The results of phonon calculation yield the eigenvalue ω_m^2, which describes a phonon frequency.

2.8.2 Born criterion

The other way to examine the structure's stability of the crystals system under pressure is used the Born criterion. In 1937, Born proposed his theory which based on the fact that a liquid differs from a crystal in having zero resistance to the shear stress. The distances between the atoms are increase due to thermal expansion, hence the restoring forces between the atoms are reduced, and therefore the shear elastic moduli decrease with the rising temperature. The softening of the shear moduli leads to a mechanical instability of the solid structure and finally lead to a collapsing of the crystal lattice at some temperature. The elastic behaviors of a lattice are described by its matrix of second-order elastic constant:

$$C_{ij} = \frac{1}{V_0}\left(\frac{\partial^2 E}{\partial\varepsilon_i \partial\varepsilon_j}\right), \tag{2.53}$$

where E is the energy of the crystal, V_0 its equilibrium volume and ε denotes a strain. The stiffness matrix has size 6×6 and is symmetric. The number of independent elastic constant can be reduced by adding symmetry constrains of the crystal class. For arbitrary homogeneous deformation by an infinitesimal strain, the energy of crystal can be written as follows;

$$E = E_0 + \frac{1}{2}V_0\sum_{i,j=1}^{6} C_{ij}\varepsilon_i\varepsilon_j + O(\varepsilon^3)\,. \tag{2.54}$$

There are two conditions to determine the stability of crystal structure. First, all of its phonon modes have positive frequencies for all wave vectors so called dynamical stability. Second, the elastic energy, given by Eq. (2.54) is always positive. The latter condition is called the elastic stability condition. For the example, in the case of cubic crystals, the conditions of stability reduce to a simple form;

$$C_{11} - C_{12} > 0; C_{11} + 2C_{12} > 0; C_{44} > 0\ . \tag{2.55}$$

However, the stability criteria must be modified when the solid is subject to an external load. The Born criterion under high pressure condition for tetragonal and hexagonal system in this work is shown as follows [19, 20];

$$C_{44}-P>0, C_{66}-P>0, C_{11}-C_{12}-2P>0$$

and

$$(C_{33}-P)(\mathrm{C}_{11}+\mathrm{C}_{12})-2(C_{13}+P)^2>0\,. \tag{2.56}$$

2.8.3 Molecular dynamic (MD)

Although the DFT is fairly popular and powerful for solving condensed matter system but it has a limitation. It is keep in mind that DFT calculation is performed under extremely 0 K. Therefore, the optimized structure from our calculation is obtained under unrealistic thermodynamic condition. In order to include temperature effect on solid system, MD is introduced in this work. It is well know that the effect of temperature are crucial for nucleus movement, the effect of temperature on the motion of nuclei has been included in order to predict the evolution of the structure at non-zero temperature. In MD calculation, the motions of the nucleus were examined by the force acting on individual nuclei which can be written as follows;

$$\mathbf{F}_I=-\frac{\partial\varepsilon}{\partial\mathbf{R}_I}, \tag{2.57}$$

where R_{I} is a nuclei position. The total energy, ε, can be expressed as

$$\varepsilon=\langle\psi|\hat{H}|\psi\rangle, \tag{2.58}$$

where ψ represent the Kohn-Sham orbital. By substitute Eq. (2.58) into Eq. (2.57) we get:

$$\begin{aligned}\mathbf{F}_I&=-\left\langle\psi\left|\frac{\partial\hat{H}}{\partial\mathbf{R}_I}\right|\psi\right\rangle-\left\langle\frac{\partial\psi}{\partial\mathbf{R}_I}\left|\hat{H}\right|\psi\right\rangle-\left\langle\psi\left|\hat{H}\right|\frac{\partial\psi}{\partial\mathbf{R}_I}\right\rangle\\&=-\left\langle\psi\left|\frac{\partial\hat{H}}{\partial R_I}\right|\psi\right\rangle-\varepsilon\left\langle\frac{\partial\langle\psi|\psi\rangle}{\partial R_I}\right\rangle\\&=-\left\langle\psi\left|\frac{\partial\hat{H}}{\partial R_I}\right|\psi\right\rangle,\end{aligned} \tag{2.59}$$

where the normalized condition is $\langle \psi | \psi \rangle = 1$.

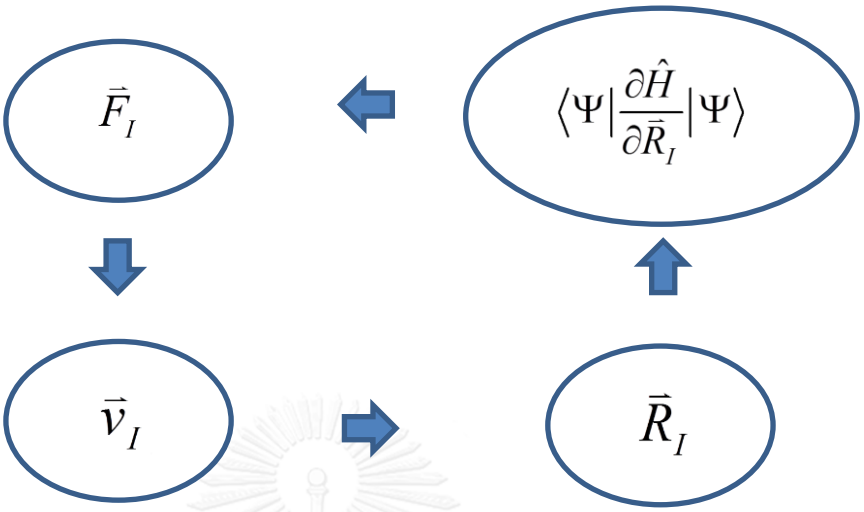

Figure 6: Diagram of Molecular dynamics (MD) method.

DFT calculation in MD method through Hellman-Feynman theorem was shown in Fig. 6. First, the optimization calculation give the ground state Kohn-Sham orbital so the force act on nuclei were obtain by Eq. 2.59. Second, the Newton's equation, $F_I = Ma_I$, was applied to obtain the acceleration. The velocity and position of nuclei were computed by integrated the acceleration once and twice, respectively. Finally, the temperature of the system can be described by the Maxwell-Boltzmann distribution as following,

$$\frac{1}{2} m v_I^2 = \frac{3}{2} N k_B T \,, \tag{2.60}$$

where k_B is the Boltzmann constant. The system will evolve until the temperature of the system is converted.

Chapter 3
Structure properties and stabilities

The II-VI ternary alloys ZnO_xS_{1-x} and ZnO_xSe_{1-x} are unable to synthesize yet due to their solubility limit [11]. In this work, we compared the total enthalpy of five different structures, namely, Chalcopyrite ($I\bar{4}2d$), Rocksalt ($Fm3m$), Zincblende ($F\bar{4}3m$), Wurtzite ($P6_3mc$) and CuAu-I ($P\bar{4}m2$) at various pressures. The symbols in parentheses after the structure names stand for space group symmetry symbol following the International Tables for Crystallography. All of the candidate structures were shown in Fig. 7. In order to investigate the structure properties and their stabilities, the lattice parameters have to be computed due to the fact that there is no experimental result yet. We applied the Vegard's law to ternary alloy systems, which is, $a(A_{1-x}B_xC)_{alloy} = (1-x)a_{AC} + xa_{BC}$, where AC stand for ZnO and BC stand for ZnS or ZnSe, to obtain the initial value of lattice parameter of all structures at 0 GPa condition. All of the lattice parameters were optimized to provide more accurate crystal structures properties. Besides, the optimized structure at high pressure was calculated to obtain the high-pressure structure properties and their corresponding stability such as bulk modulus, phonon dispersion and electronic structure. The results will yield the condition for synthesize ternary alloy II-VI films and also their corresponding properties of high pressure phase structure.

For O doped in II-VI case, previous researchers reported two different structures namely Wurtzite and Zincblende, which obtained from two different conditions in the film growth processes [10,11]. To investigate the lowest enthalpy of crystal structure, Wurtzite, Zincblende and Rocksalt structures were optimized to improve structure at 0-50 GPa conditions. It is note here that Rocksalt structure is common high-pressure structure phase of II-VI semiconductor, which was included to consider the new phase of Wurtzite and Zincblende structures at high-pressure condition. Not only the total enthalpies of all structures were calculated but also the structure stability and corresponding electronic structures at high-pressure conditions were presented here for the first time. In this chapter, we present the computational

detail, the calculated enthalpies, bulk modulus and phonon dispersion of all structure at ambient as well as high-pressure conditions to reveal the most stable structure at these conditions.

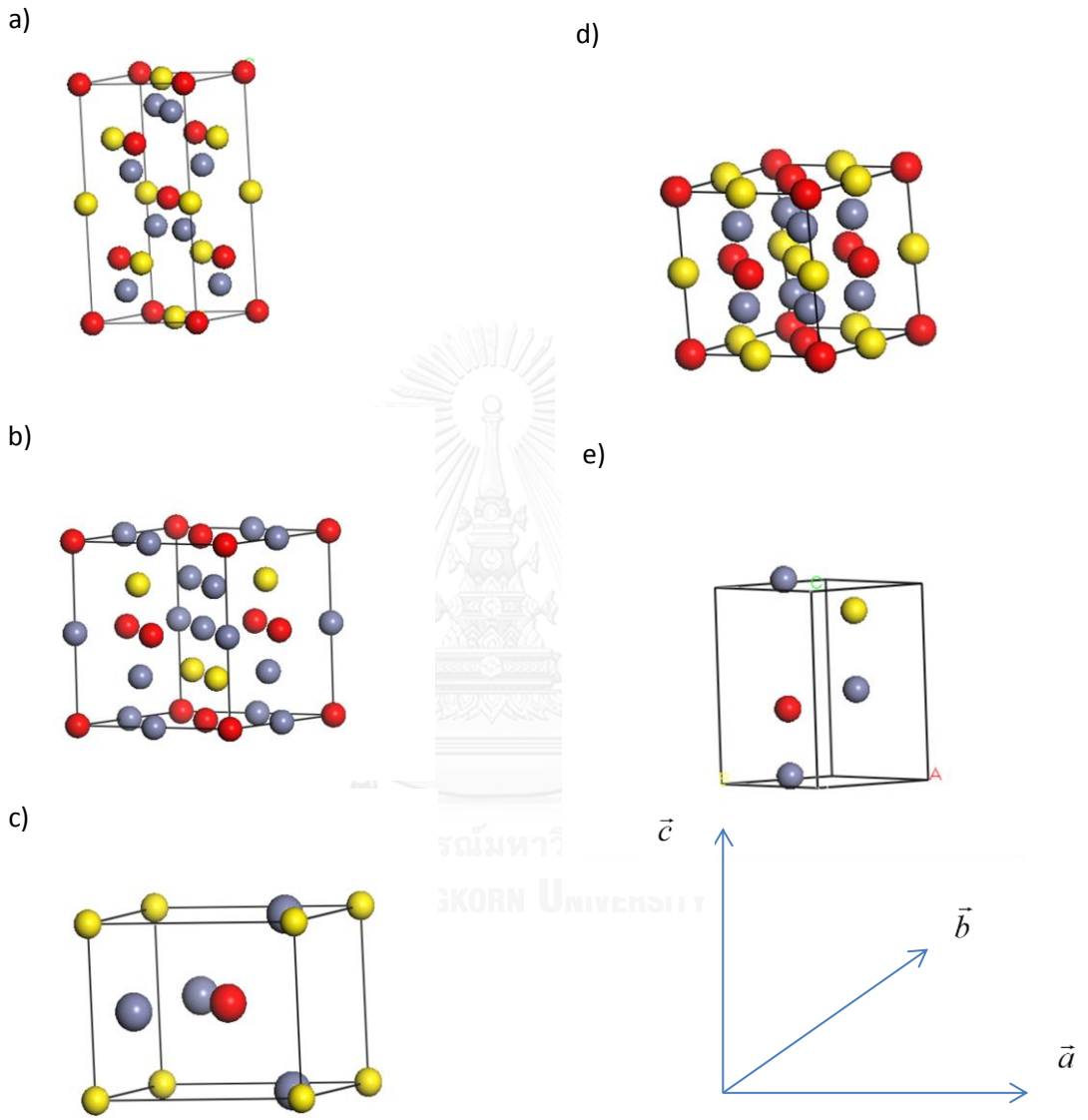

Figure 7: The five possible structures for $ZnO_{0.5}S_{0.5}$ and $ZnO_{0.5}Se_{0.5}$ a) Chalcopyrite b) Zincblende c) CuAu-I d) Rocksalt and e) Wurtzite.

In this work, the self-consistent field (SCF) method in Cambridge Serial Total Energy Package (CASTEP) code [21, 22] with plane wave basis set were used to investigate the structural properties and stability of $ZnO_{0.5}S_{0.5}$, $ZnO_{0.5}Se_{0.5}$ and $Zn_{16}O_1S_{15}$ at high-pressure condition. All the calculations performed in this chapter

are based on DFT using GGA scheme.

In order to compare our calculation results with the experiment, we computed the properties of II-VI semiconductors such as ZnO, ZnS and ZnSe in Wurtzite and Zincblende structures at ambient condition using GGA as exchange-correlation functional. The convergence tests of energy cutoff and k-point have been done. The calculation results compared with the others experimental works were shown in table 1. The results yield that our calculated lattice constants are only difference from the experimental less than 2%. For electronics properties, it is well known that the energy gap in GGA scheme is under estimate so our electronic properties calculation can only suggest the trend but not an exact value. However, in this work the hybrid functional HSE06 was introduced to obtain more accurate electronic properties.

Table 1: The optimized lattice parameter and energy gap of II-VI semiconductors compared with the experimental results.

	ZnO		ZnS		ZnSe
Lattice constant (Å)	Wurtzite	Zincblende	Wurtzite	Zincblend	Zincblend
a	3.28, 3.25[23, 24]	4.620, 4.60[23]	3.842, 3.811[23]	5.438, 5.42[23]	5.692, 5.67[23]
c	5.29, 5.20[25]		6.301, 6.234[23]		
Energy gap (eV)	1.157, 3.2[23]	0.646, 3.28[25]	2.172, 3.68[23]	2.109, 3.911[23, 24]	1.304, 2.7[23, 24]

For phonon dispersion calculation, CASTEP provide two powerful tools to obtain phonon dispersion of solid system namely linear response and finite displacement methods. We compared the phonon dispersion calculations results of both linear response and finite displacement methods of ZnO in Wurtzite structure in Fig. 8. According to Fig. 8, the phonon calculations results from both methods yield similar thread. Both linear response and finite displacement methods provided non-imaginary frequencies. This result is good agreement with experimental result that ZnO can be synthesized in Wurtzite structure at ambient condition. Unfortunately, the linear response in CASTEP code is only supported norm-conserving pseudopotential which the researchers proposed that required more computing power beyond the

available resource since it required more energy cutoff to converge than the ultrasoft pseudopotential in finite displacement method. In this work, we used the finite displacement method to investigate the phase stability.

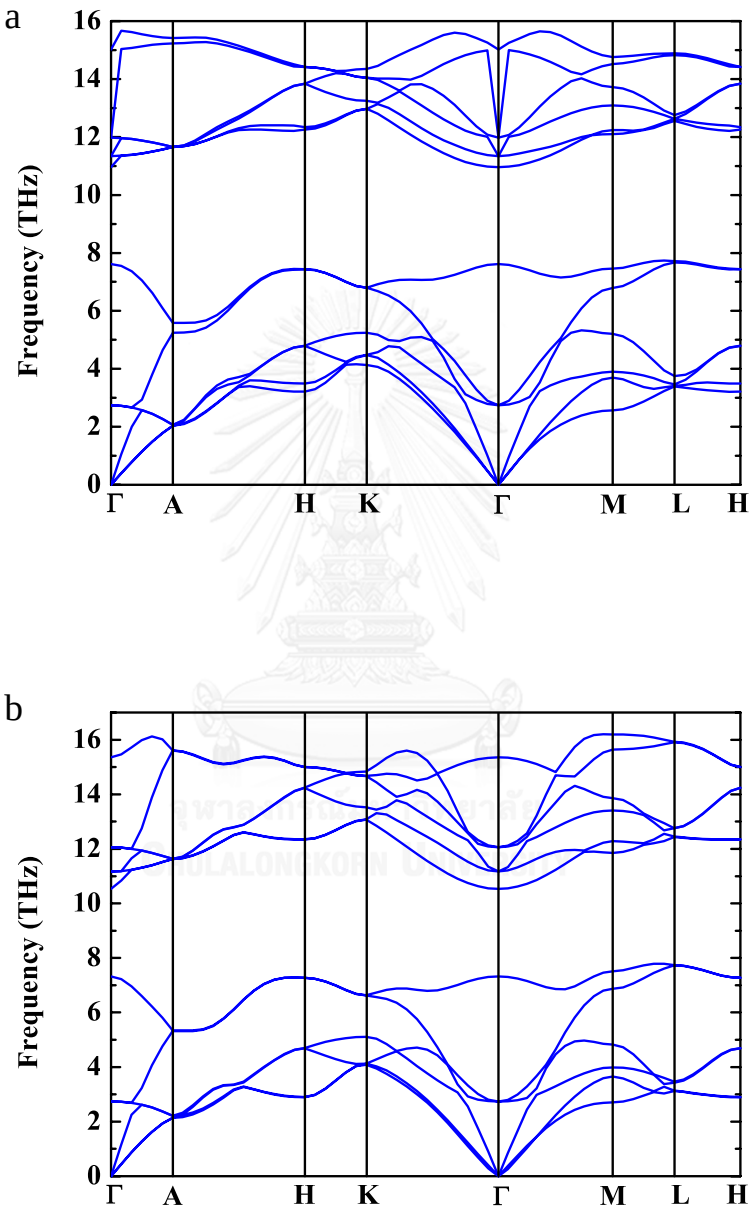

Figure 8: The phonon dispersion of ZnO in Wurtzite structure by a) linear response and b) finite displacement methods.

3.1 The structure of $ZnO_{0.5}S_{0.5}$ and $ZnO_{0.5}Se_{0.5}$

Even the higher cutoff energy (more term required in plane wave basis set) leads to more accurate result but they also consume significant computational resource since the convergence test has to be done to optimize resource. The energy convergence tests were calculated by comparing total energy of plane wave with cutoff energy in all structures. The cutoff energy convergence test of $ZnO_{0.5}S_{0.5}$ and $ZnO_{0.5}S_{e0.5}$ in Chalcopyrite and CuAu-I structures were shown in Fig. 9 and 10 respectively. In addition, the k-points convergence tests are performed in all structures. The energy versus number of k-points of $ZnO_{0.5}S_{0.5}$ and $ZnO_{0.5}S_{e0.5}$ in Chalcopyrite and CuAu-I were shown in Fig. 11 and 12 respectively. The lattice parameters and calculations setting of all structures are listed in table 2.

Table 2: The lattice parameter, energy cutoff and k-points of five structures were shown.

Structure	a (Å)	c (Å)	Energy cutoff (eV)	k-points
Chalcopyrite	5.0411	10.055	550	8×8×4
Rocksalt	5.9155		550	6×6×6
Zincblende	5.9633		600	6×6×6
Wurtzite	3.5760	5.8394	550	6×6×6
CuAu-1	3.6256	4.8386	700	6×6×6

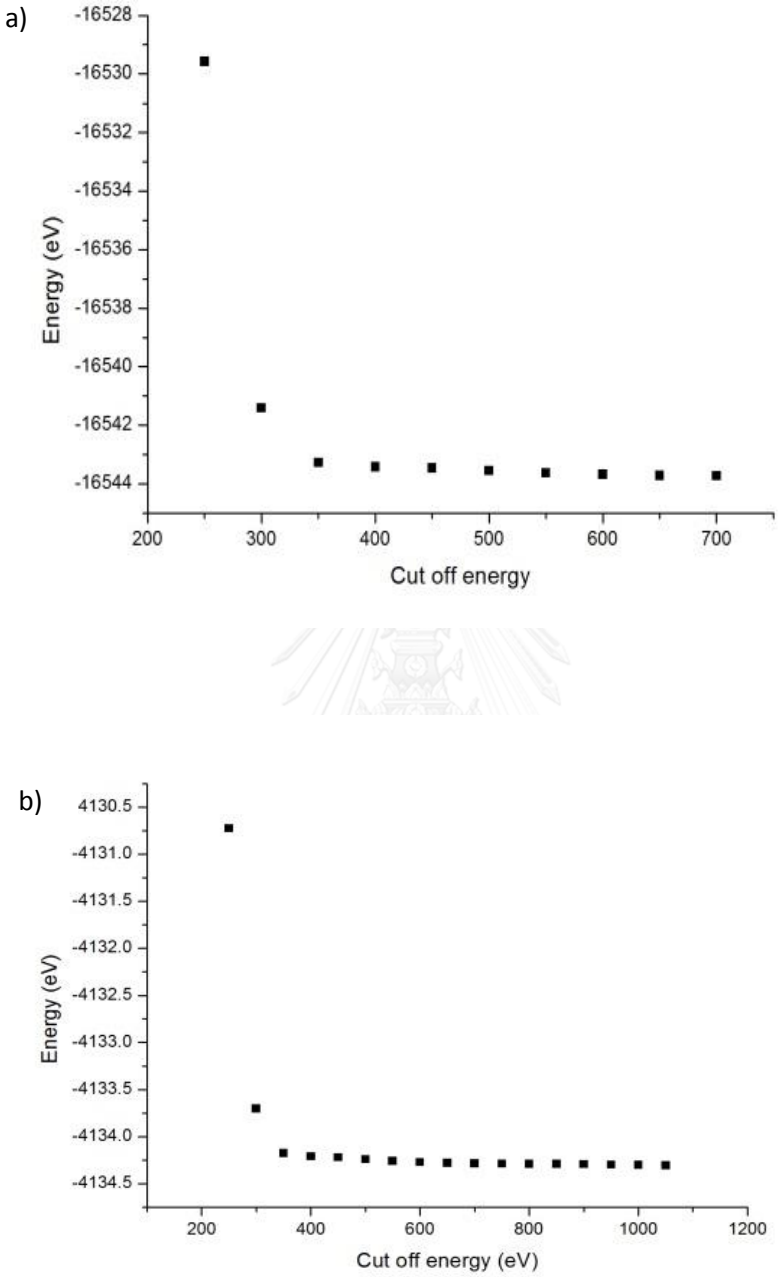

Figure 9: The cutoff energy convergence test of $ZnO_{0.5}S_{0.5}$ in a) Chalcopyrite and b) CuAu-I structures.

a)

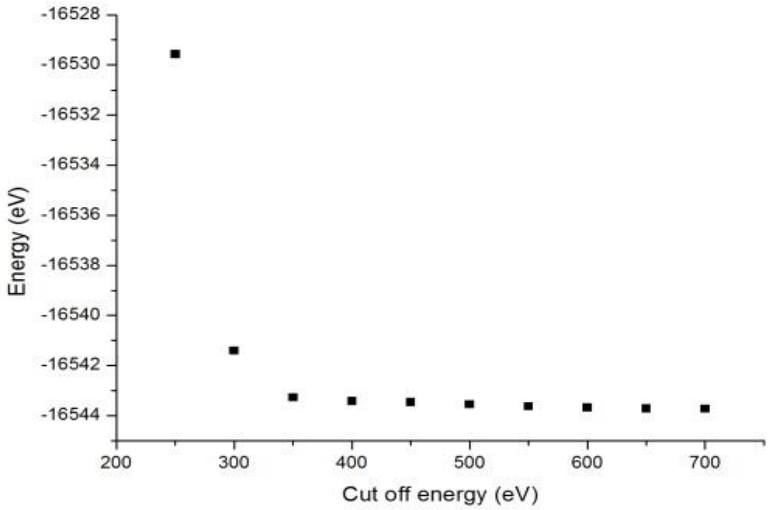

b)

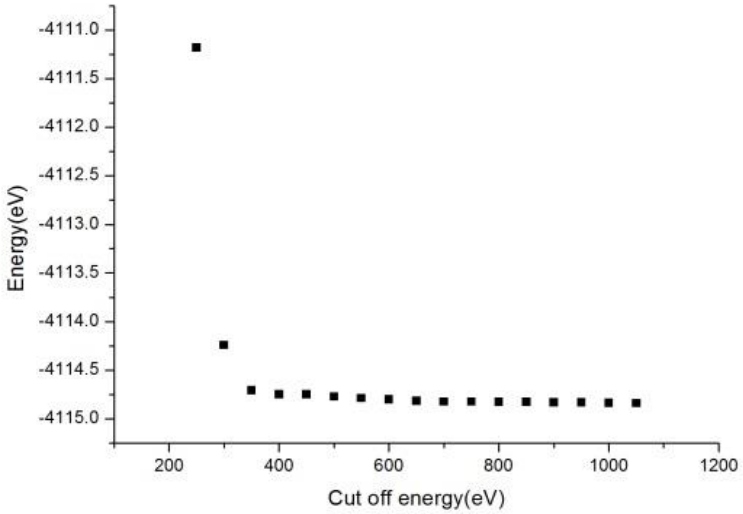

Figure 10: The cutoff energy convergence test of $ZnO_{0.5}Se_{0.5}$ in a) Chalcopyrite and b) CuAu-I structures.

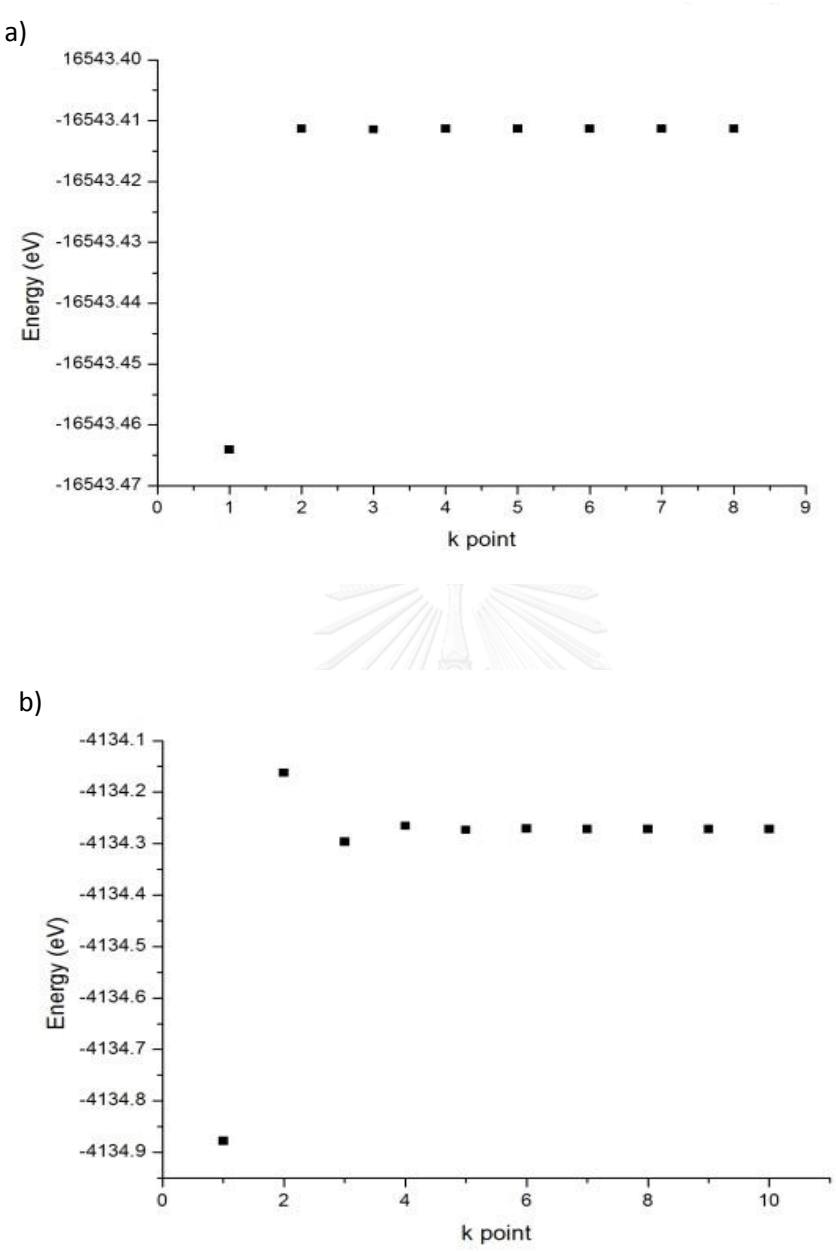

Figure 11: The k-point convergence test of $ZnO_{0.5}S_{0.5}$ in a) Chalcopyrite and b) CuAu-I structures.

a)

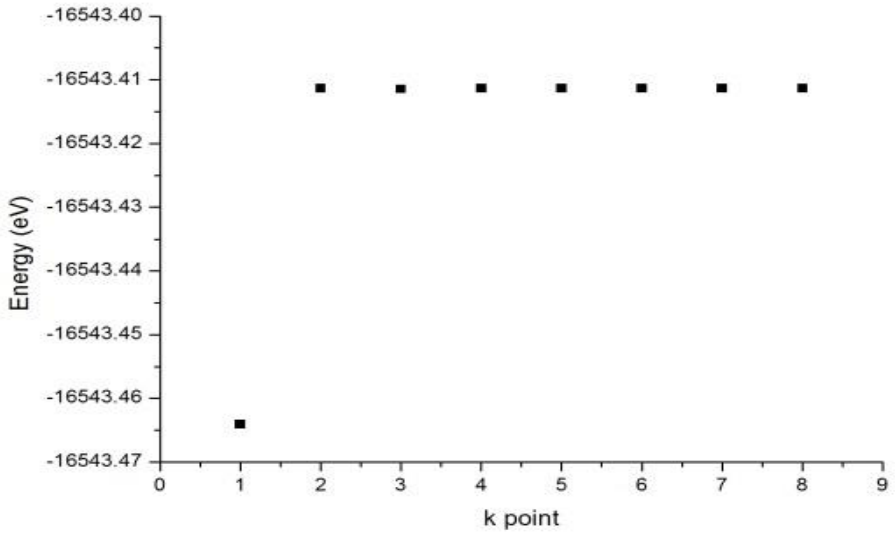

b)

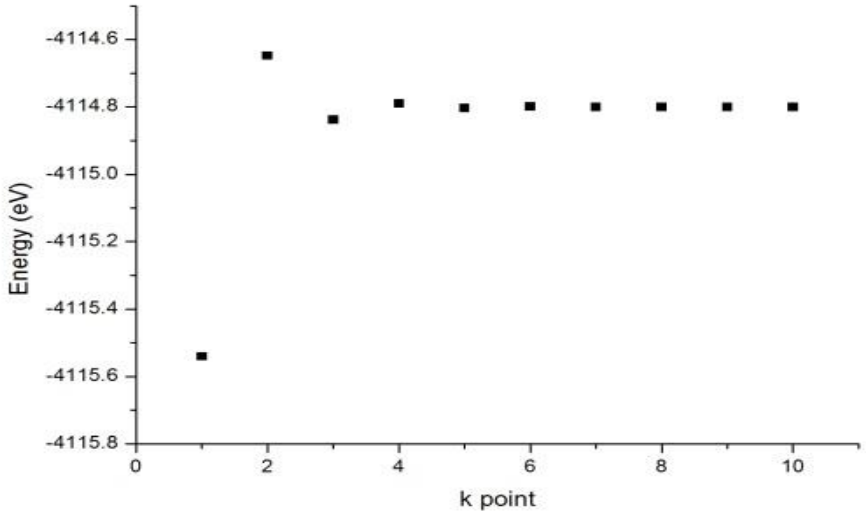

Figure 12: The k-point convergence test of $ZnO_{0.5}Se_{0.5}$ in a) Chalcopyrite and b) CuAu-I structures.

3.2 The structure stability of $ZnO_{0.5}S_{0.5}$ and $ZnO_{0.5}Se_{0.5}$

In order to investigate the most stable structure at ambient and also high-pressure condition, we compared total enthalpy of the five structures at various pressures. The total enthalpies differences from Chalcopyrite structure in $ZnO_{0.5}S_{0.5}$ and $ZnO_{0.5}Se_{0.5}$ with various pressures were shown in Fig. 13a and 13b. By considering the total enthalpy differences between the Chalchopyrite and the others structures, we found that the lowest enthalpy structure of both $ZnO_{0.5}S_{0.5}$ and $ZnO_{0.5}Se_{0.5}$ at low-pressure regime is the Chalchopyrite and then they transform to CuAu-I at high-pressure condition. The transition pressures are at 27 GPa and 30 GPa for $ZnO_{0.5}S_{0.5}$ and $ZnO_{0.5}Se_{0.5}$ respectively.

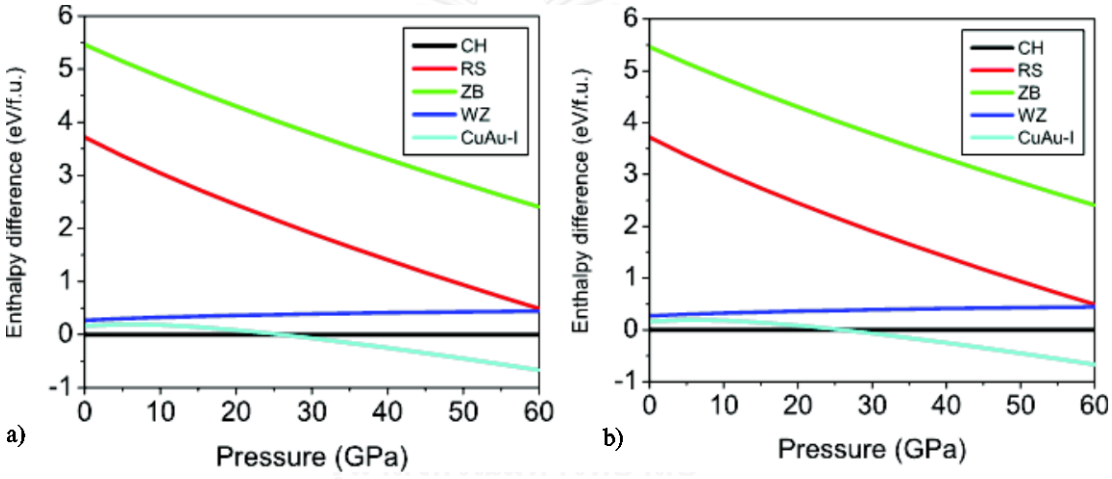

Figure 13: The total enthalpies difference compare with Chalcopyrite structure per formulae unit versus pressure of a) $ZnO_{0.5}S_{0.5}$ and b) $ZnO_{0.5}Se_{0.5}$.

Not only the lowest enthalpy was used to reveal the stable structure at any pressure but also the necessary elastic stiffness constant conditions have to be considered in mechanical stability point of view. We perfumed elastic stiffness constants calculation on both Chalcopyrite and CuAu-I structures with various pressures. The bulk modulus and elastic stiffness constants are shown in table 3 The Born criterion to be stable structure in both Chalcopyrite, CuAu-I (tetragonal) and Wurtzite (hexagonal) are $C_{11} > |C_{12}|; 2C_{13}^2 < C_{33}(C_{11}+C_{12}); C_{44} > 0; C_{66} > 0$ for 0 GPa and Eq. (2.56) for applied pressure conditions respectively. According to table 3, the Chalcopyrite structures in both $ZnO_{0.5}S_{0.5}$ and $ZnO_{0.5}Se_{0.5}$ satisfied the Born criterion

at 0 GPa and also satisfied lowest necessary conditions for Born criterion at high-pressures conditions up to 10 GPa, so Chalcopyrite structure can be the stable structure up to 10 GPa. On the other hand, CuAu-I provided negative value in C_{66} in both $ZnO_{0.5}S_{0.5}$ and $ZnO_{0.5}Se_{0.5}$ structures at 25-35 GPa, which are not satisfaction for necessary mechanical stability conditions in solid. Therefore, the structures of II-VI ternary alloys in this work may be Chalcopyrite structure up to 10 GPa but the high-pressure CuAu-I phase is not a stable structure due to mechanical stability conditions. In order to verify this, further calculations have been performed.

One of the most powerful tools to observe the dynamical stability of any structure is phonon dispersion calculation. The main idea of this tool is that the negative phonon frequencies do not contain in phonon dispersion of stable structure. In order to check the dynamical stability of the candidate structures, the phonon dispersion calculation were performed at 0-30 GPa for Chalcopyrite and 25-35 GPa for CuAu-I respectively. The phonon dispersions of $ZnO_{0.5}S_{0.5}$ and $ZnO_{0.5}Se_{0.5}$ in both candidate structures at various pressures were shown in Fig. 14 for $ZnO_{0.5}S_{0.5}$ and Fig. 15 for $ZnO_{0.5}Se_{0.5}$. The high symmetry point of both Chalcopyrite and CuAu-I were shown in Table 4. According to Fig. 14a, the Chalcopyrite $ZnO_{0.5}S_{0.5}$ phonon dispersion shows the phase transition signal with increase in pressure through softening of acoustic phonon around M and R points. Nevertheless, up to 30 GPa, it never reaches negative value. For the Chalcopyrite $ZnO_{0.5}Se_{0.5}$ (see Fig. 15a), the phonon dispersion shows softening of acoustic mode around X and Z points but non-negative frequencies occurred.

Table 3: The elastic stiffness constant and bulk modulus of Chalcopyrite and CuAu-I structure with various pressures of $ZnO_{0.5}S_{0.5}$ and $ZnO_{0.5}Se_{0.5}$.

$ZnO_{0.5}S_{0.5}$ Chalcopyrite							
Pressure (GPa)	C_{11}	C_{12}	C_{13}	C_{33}	C_{44}	C_{66}	B (GPa)
0	145.24935	100.85090	104.73770	152.09275	66.44435	57.53515	117.94341
10	178.76330	141.44775	146.75775	184.96845	58.49910	46.95335	156.64997
20	208.98915	186.08790	192.54785	233.53605	47.97290	38.35075	196.99682
30	235.20130	230.88105	236.50550	278.46490	40.33175	33.56435	232.72941
$ZnO_{0.5}S_{0.5}$ CuAu-I							
25	308.88098	196.47036	162.06800	127.62283	26.72024	-1.89740	117.96243
30	357.34535	224.17780	172.84955	145.58930	20.45690	-36.35970	137.39176
35	395.23555	248.71070	184.01255	170.46665	18.17965	-65.13380	168.99181
$ZnO_{0.5}Se_{0.5}$ Chalcopyrite							
Pressure (GPa)	C_{11}	C_{12}	C_{13}	C_{33}	C_{44}	C_{66}	B (GPa)
0	84.46470	60.30870	48.74905	117.06870	44.54605	43.18810	66.31064
10	143.74795	115.69475	120.95565	163.85050	31.46395	46.72340	128.23400
20	198.69780	177.31465	186.41870	232.39590	52.58430	49.64665	187.95324
30	207.62255	199.50615	207.22950	256.16495	60.24755	63.20915	203.26761
$ZnO_{0.5}Se_{0.5}$ CuAu-I							
25	302.79335	196.08170	152.03135	126.79065	-1.23465	-40.45170	117.96243
30	342.06010	218.67255	161.49445	150.94575	2.31100	-81.60795	149.91850
35	372.19530	237.12085	173.93905	176.32665	14.95200	-204.1679	176.28382

Beside, CuAu-I structure yielded phonon hardening sign (see Fig. 14b and 15b) in both $ZnO_{0.5}S_{0.5}$ and $ZnO_{0.5}Se_{0.5}$.To conclude, in the low pressure regime, We found no imaginary phonon frequency and no Born criteria violation elastic stiffness constants up to 10 GPa for Chalchopyrite. However, for CuAu-I, there exist the unsatisfactory elastic stiffness constant, C_{66}. Therefore, Chalchopyrite is the only stable structure of $ZnO_{0.5}S_{0.5}$ and $ZnO_{0.5}Se_{0.5}$ at ambient which is in excellent agreement with the others researchers [6–8].

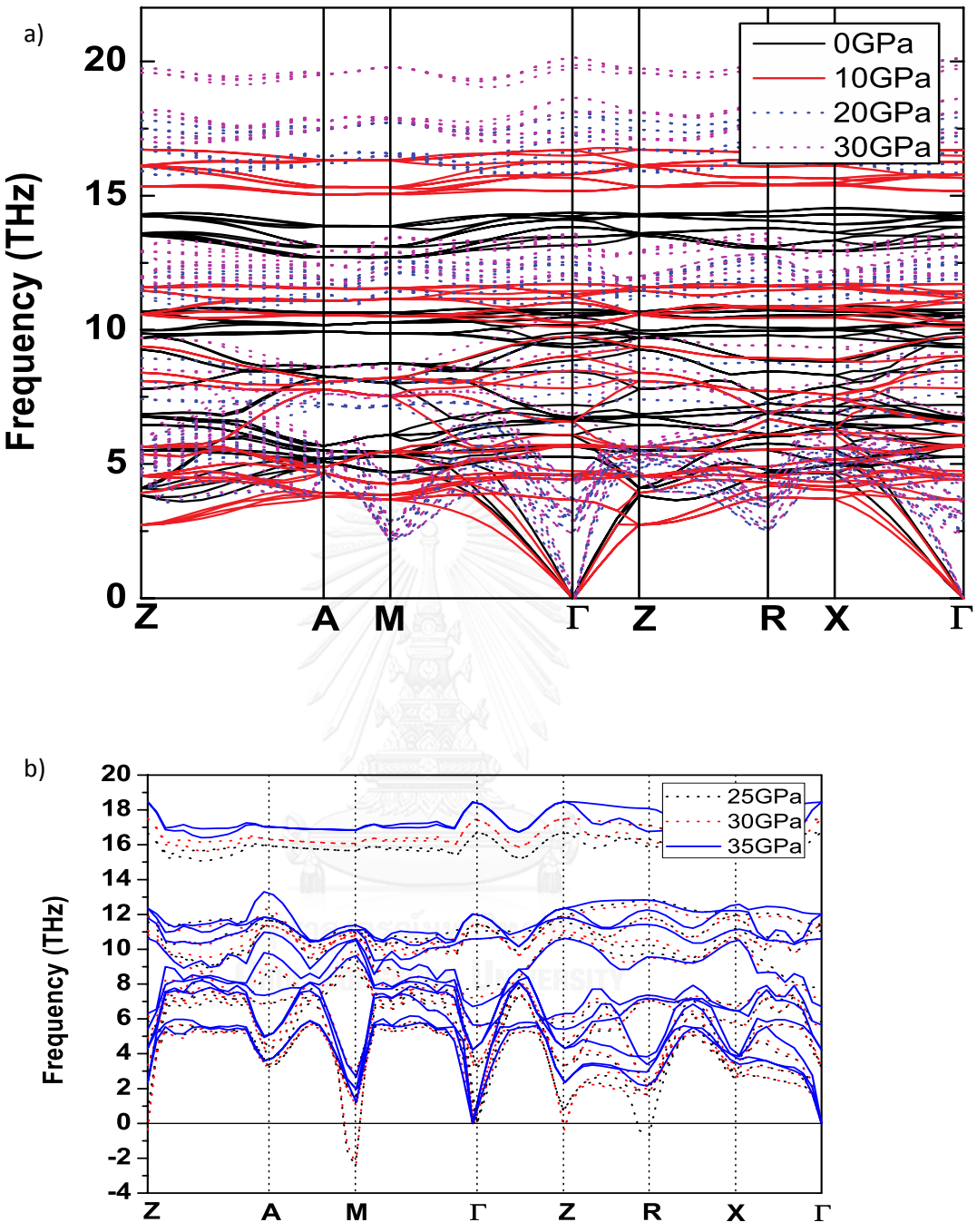

Figure 14: The phonon dispersion of $ZnO_{0.5}S_{0.5}$ of a) Chalcopyrite and b) CuAu-I structures with various pressures.

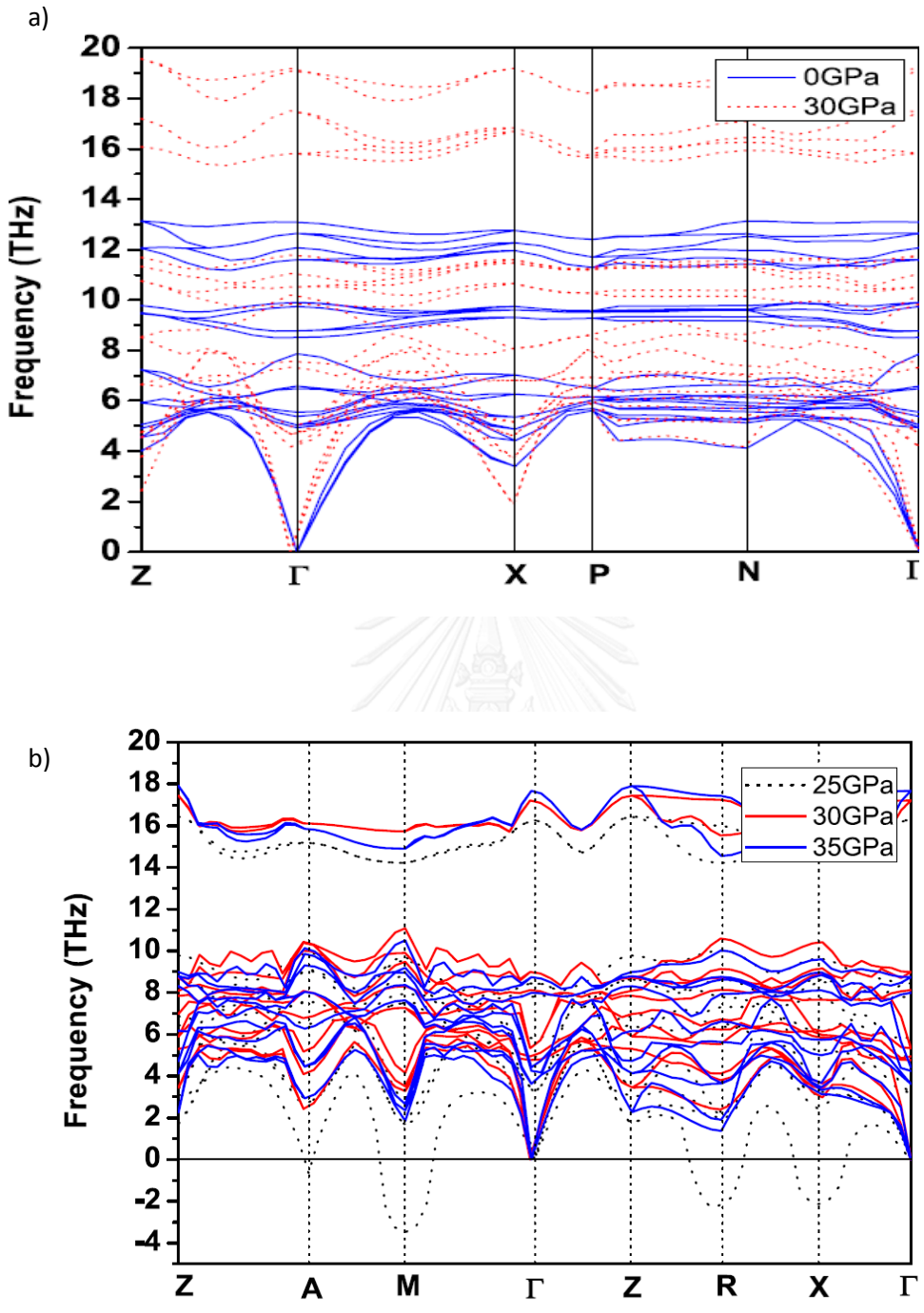

Figure 15: The phonon dispersion of $ZnO_{0.5}Se_{0.5}$ of a) Chalcopyrite and b) CuAu-I structure with various pressures.

Table 4: The symmetry point of a) Chalcopyrite and b) CuAu-I structures.

a)

Lable	Coordinates
Z	$\frac{1}{2}$ $\frac{1}{2}$ $-\frac{1}{2}$
Γ	0 0 0
X	0 0 $\frac{1}{2}$
P	$\frac{1}{4}$ $\frac{1}{4}$ $\frac{1}{4}$
N	0 $\frac{1}{2}$ 0

b)

Lable	Coordinates
Z	0 0 $\frac{1}{2}$
A	$\frac{1}{2}$ $\frac{1}{2}$ $\frac{1}{2}$
M	$\frac{1}{2}$ $\frac{1}{2}$ 0
Γ	0 0 0
R	0 $\frac{1}{2}$ $\frac{1}{2}$
X	0 $\frac{1}{2}$ 0

To obtain more evidence for our calculations, the MD calculations were established. NPT [26] Gamma-point (Γ-point) MD calculations were employed for the Chalcopyrite structure (Zn 108, O and S 54 atoms) and CuAu-I structure (Zn 54, O and Se 27 atoms) systems at 300 K under 30 GPa. The converged results from MD calculations of Chalcopyrite and CuAu-I structures of $ZnO_{0.5}S_{0.5}$ at 30 GPa and 300 K are shown in Fig. 16b and 16d, respectively. By comparing with their respective initial structures Fig. 16a and 16c, Zn (grey) S (yellow) and O (red) atoms fluctuate about their equilibrium point owing to the temperature effect and this result converged within 1 ps simulation time, nevertheless they are still in the same crystal plane as the initial supercell. In contrast, in the case of CuAu-I structure, Zn (grey) atoms in [100] and [010] plane in the final supercell (see Fig. 16d) are distorted and tend to change the supercell into another structure after 5 ps of MD calculation time which shows that this structure is not vibrational stable. This indicates that the Chalcopyrite structure were stable at 30 GPa and 300 K even adding the temperature effect by MD calculation. However, combining these results with those of the phonon dispersion and the Born criteria, these are the strong evidences enable us to conclude that the Chalcopyrite structure is the most stable structure up to only 10 GPa due to elastic constant stability condition. These results also agree with the ternary alloy such as $I-III-VI_2$ and $II-IV-V_2$ they tend to be in Chalcopyrite structure at ambient condition at room temperature [27]. In addition, the phonon softening and decreasing

of C_{66} with the increasing pressure of the Chalcopyrite phase show the possibility of phase transition at higher pressure.

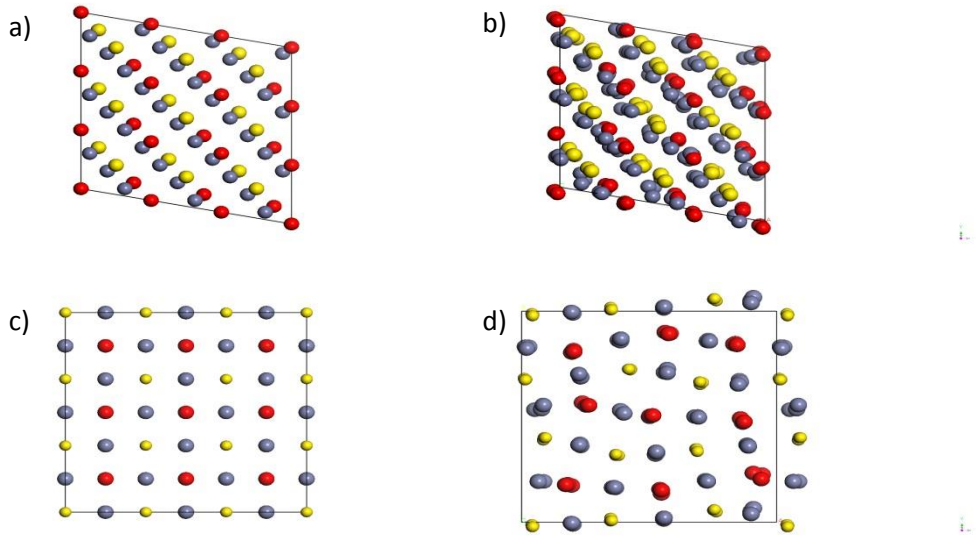

Figure 16: a) The initial optimum supercell of $ZnO_{0.5}S_{0.5}$ in Chalcopyrite structure at 0 GPa and 0 K b) The final supercell at 30 GPa and 300 K c) The initial optimized supercell of $ZnO_{0.5}S_{0.5}$ in CuAU-I structure at 30 GPa and 0 K and d) The final supercell at 30 GPa 300 K.

Not only the structure stability and properties of II-VI ternary alloys were investigated but phase transition also were included in this work. Rocksalt structure, the common high-pressure phase of II-VI semiconductors, is examined due to its enthalpy is lower than Chalcopyrite structure at 70 GPa. The phonon dispersion were calculated at 70 GPa. The result revealed that Rocksalt structure was unstable at high-pressure regime. The phonon dispersion of Rocksalt structure at 70 GPa was shown in Fig. 17.

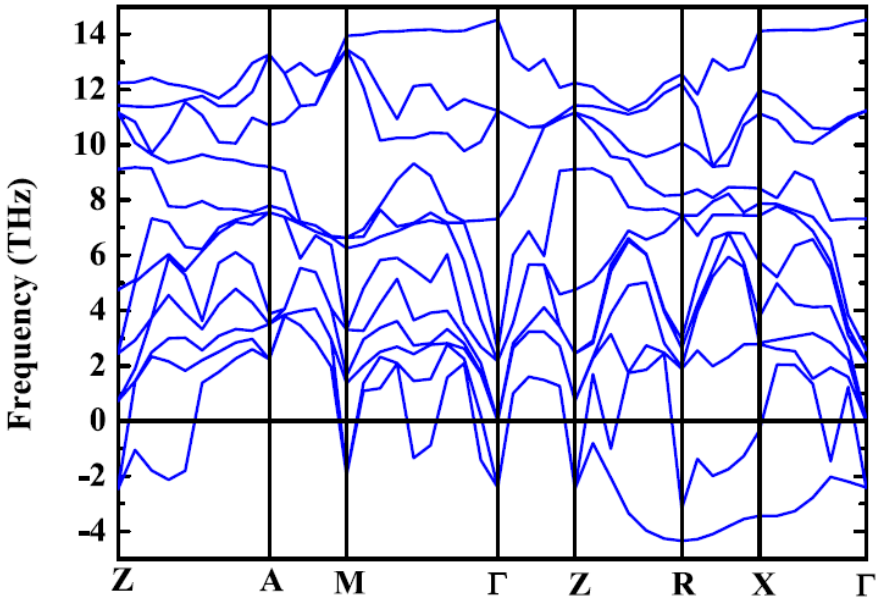

Figure 17: The phonon dispersion of Rocksalt structure at 70 GPa condition.

3.3 The structure stability of O doped in ZnS

Two dilute O-doped ZnS − *i.e.* $Zn_{16}O_1S_{15}$ − systems are modeled by substituting an S atom of 2 × 2 × 1 Zincblende and 2 × 2 × 2 Wurtzite supercells, which compose of 16 Zn and 16 S atoms, with an O atom. In addition, the energy cutoff and k-point convergences test have been done.

According to Pan *et al.* [10] and He *et al.* [11], structures of S rich O-doped ZnS are both Zincblende and Wurtzite at ambient pressure depending on sample preparations. To figure out that which one is the most stable structure of $Zn_{16}O_1S_{15}$ at a given pressure, we compared the enthalpy/formula of Wurtzite with that of Zincblende as a function of pressure. The result is shown in Fig. 18. At low pressure, the lowest enthalpy/formula structure is Zincblende. The Zincblende enthalpy/formula is lower than that of Wurtzite about 0.238 eV/formula at 0 GPa and slightly more at higher pressure. The Wurtzite enthalpy/formula difference is fairly firm against pressure before it approaches a particular pressure at which it becomes zero, ~42 GPa. After this pressure, the Wurtzite structure is energetically more preferable than Zincblende. On the other hand, Bilge *et al.* [12] reported that ZnS crystallizes in cubic Zincblende and Wurtzite structure at ambient pressure condition. There is a phase

transition from Wurtzite to Zincblende and from Zincblende to Rocksalt under high pressure condition. As mention before, both of Zincblende and Wurtzite structures of S rich in $ZnO_{1-x}S_x$ films were observed experimentally. This can be explained by our results as follows. At ambient pressure the both of Zincblende and Wurtzite structures are stable and the energetically preferable one is the Zincblende. Thus, a difference in growing temperatures results in different crystal structures. In Pan *et al.*'s [10] work, the temperatures during annealing process were around 773-873 K. While in He *et al.*'s [11] work the temperature of the ZnS substrate was 1023 K. The thermal energy differences between these two sample preparations are in a range of 0.207 – 0.345 eV/formula, assuming that each atom gained $\frac{1}{2}k_BT$ thermal energy. This is a reason why they obtained such crystal structures.

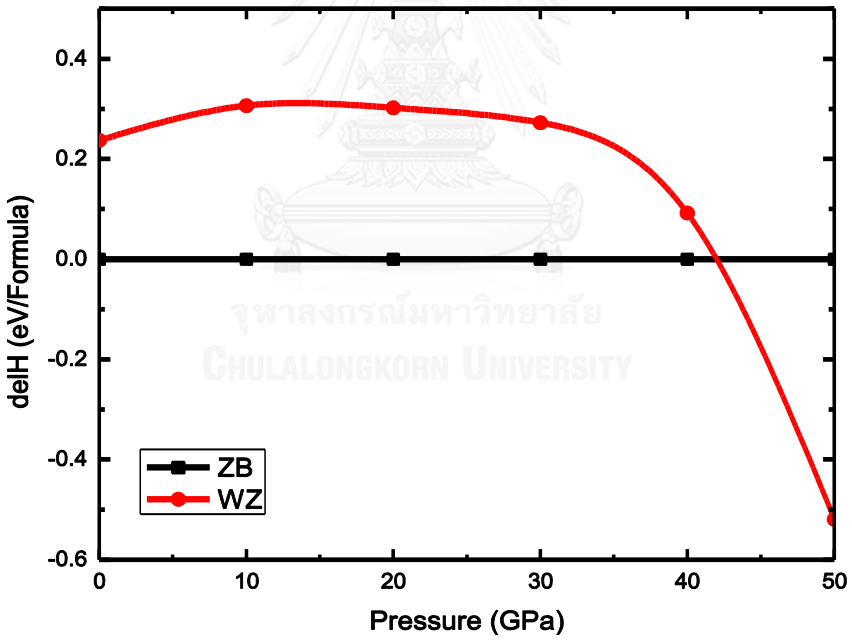

Figure 18: The total enthalpies difference compare with Zincblende structure per formulae unit of $Zn_{16}O_1S_{15}$ versus pressure.

In order to examine the mechanical and dynamical stability of both Zincblende and Wurtzite structure at a given pressure, we computed the phonon dispersion and elastic stiffness constant at a given pressure. The phonon dispersion were shown in Fig. 19 and 20 for Zincblende and Wurtzite structures respectively. The elastic stiffness constant calculations results were shown in table 5. Besides, the high symmetry point of both Zincblende and Wurtzite were shown in Table 6. For Zincblende structure, The phonon dispersion, $\omega^2(k)$, and elastic constants show that this structure is mechanical stable from 0 to 10 GPa and unstable at 20 GPa as the former reaches negative values and the latter violate the Born criteria, *i.e.* $C_{11}-C_{12}-2P=-11.32<0$, (see Fig. 19 and Tab. 5). On the other hand, Wurzite structure obeys both mechanical stability conditions at a range of pressure from 0 to 20 GPa (see Fig. 20 and Tab. 5).

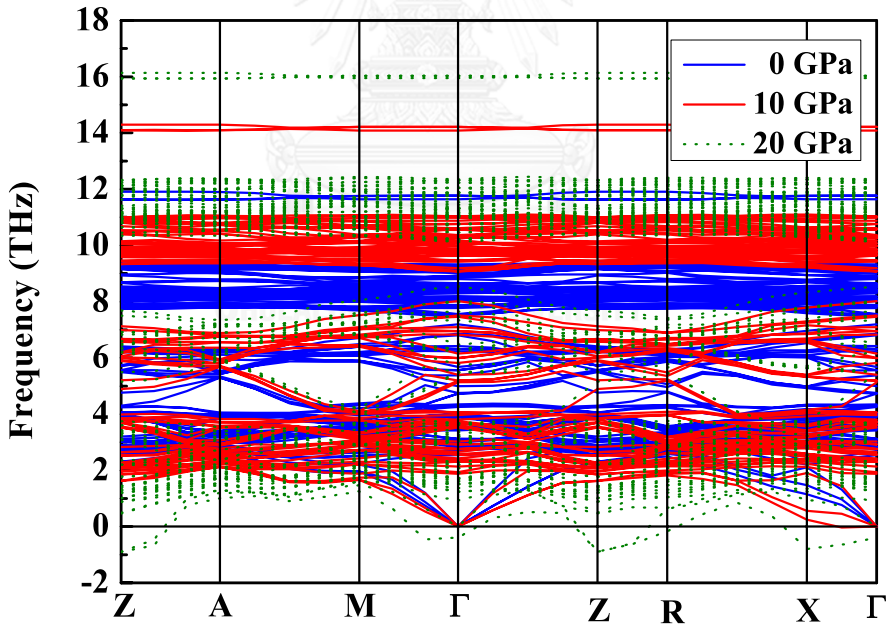

Figure 19: The phonon dispersion of $Zn_{16}O_1Se_{15}$ in Zincblende structure with various pressures.

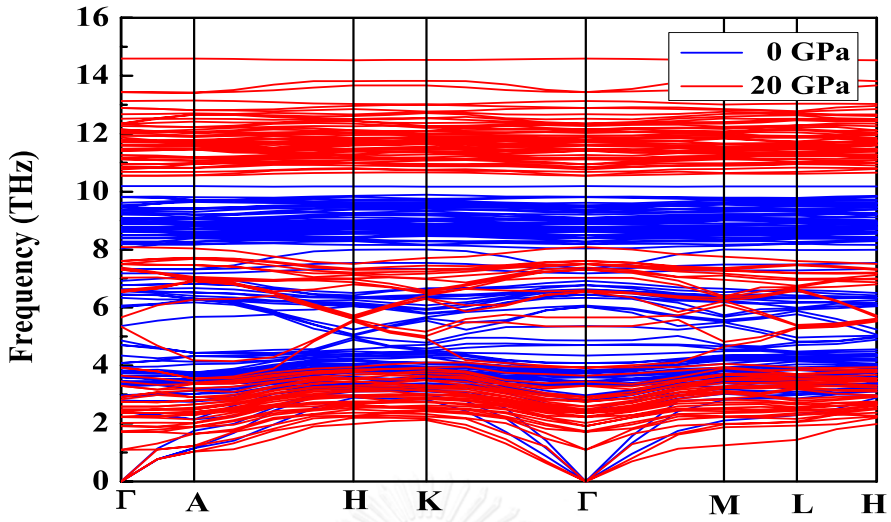

Figure 20: The phonon dispersion of $Zn_{16}O_1Se_{15}$ in Wurtzite structure with various pressures.

Table 5: The elastic stiffness constants and bulk modulus of $Zn_{16}O_1S_{15}$ with various pressures.

Zincblende							
Pressure (GPa)	C_{11}	C_{12}	C_{13}	C_{33}	C_{44}	C_{66}	B (GPa)
0	99.70	58.15	58.15	99.67	48.43	48.68	72.00
10	137.66	101.79	101.70	137.46	45.43	46.00	113.69
20	171.55	142.87	142.74	170.45	40.13	40.20	152.25
Wurtzite							
0	118.38	52.52	40.77	138.80	28.11	32.93	71.46
10	157.64	94.51	80.70	188.24	25.21	31.56	112.61
20	188.07	134.06	122.51	228.00	20.85	27.00	150.74

It is well known that Rocksalt structure is the common high-pressure phase for both Zincblende and Wurtzite structure in II-VI semiconductor. In this work, we also investigated the phase transition in O doped ZnS. The total enthalpy/formulae versus pressure were calculated comparing with low-pressure phase. The results were shown in Fig. 21. Even, the enthalpy/formulae of Rocksalt structure is the most energetically preferable structure and the phase transition from Zincblende or Wurtzite to Rocksalt occurs at around 17.5 GPa but its phonon dispersion, which is shown in Fig. 22, yield an imaginary phonon frequencies so the Rocksalt structure was excluded in this point of view.

Table 6: The symmetry point of a) Zincblende structure and b) Wurtzite structure

a)

Lable	Coordinates
Z	$0 \quad 0 \quad \frac{1}{2}$
A	$\frac{1}{2} \quad \frac{1}{2} \quad \frac{1}{2}$
M	$\frac{1}{2} \quad \frac{1}{2} \quad 0$
Γ	$0 \quad 0 \quad 0$
R	$0 \quad \frac{1}{2} \quad \frac{1}{2}$
X	$0 \quad \frac{1}{2} \quad 0$

b)

Lable	Coordinates
Γ	$0 \quad 0 \quad 0$
A	$0 \quad 0 \quad \frac{1}{2}$
H	$\frac{1}{3} \quad \frac{2}{3} \quad \frac{1}{2}$
K	$\frac{1}{3} \quad \frac{2}{3} \quad 0$
M	$0 \quad \frac{1}{2} \quad 0$
L	$0 \quad \frac{1}{2} \quad \frac{1}{2}$

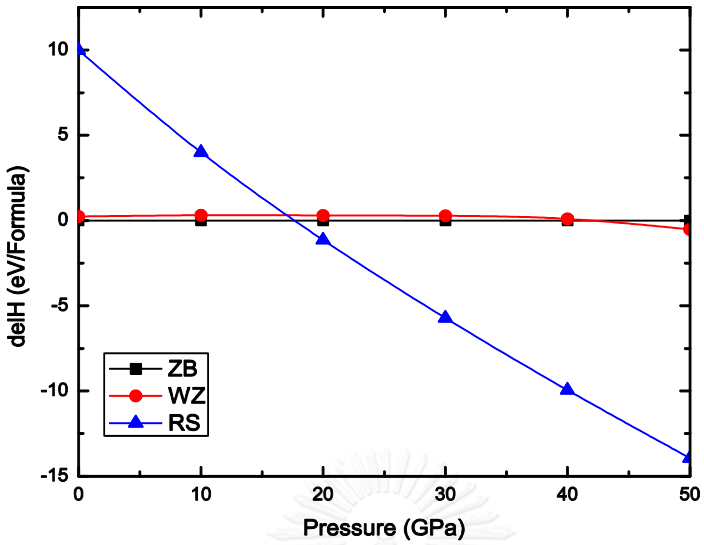

Figure 21: The total enthalpies difference compare with Zincblende structure per formulae unit of $Zn_{16}O_1S_{15}$ versus pressure.

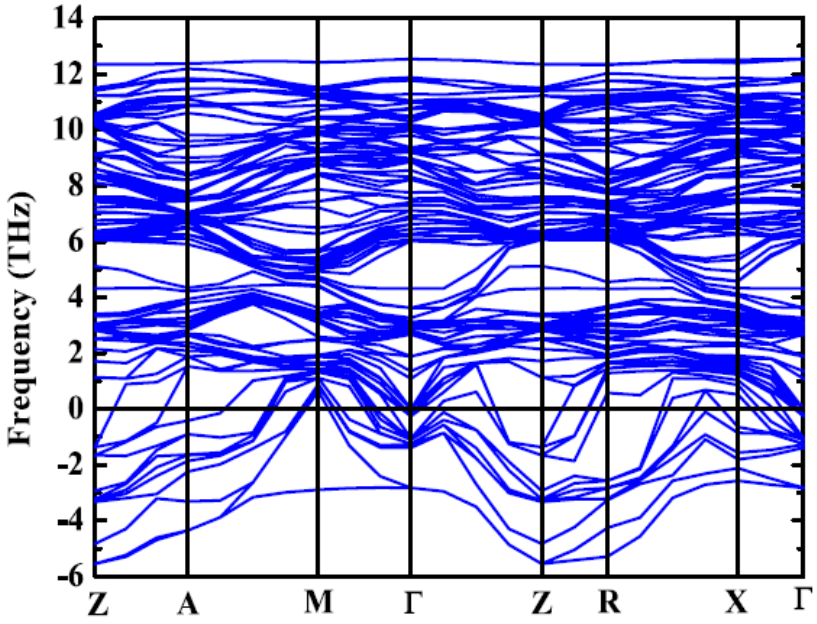

Figure 22: The phonon dispersion of Rocksalt structure at 40 GPa.

Chapter 4
ELECTRONIC PROPERTIES

II-VI wide band gap semiconductors have been used in blue-range optoelectronic device due to wide band gap. In addition, these types of semiconductors have also drawn interest for substitute in III-V, which dominate the solar cell device scene. Due to the large bowing parameter of II-VI semiconductor lead to more adjustable band gap than III-V groups [5,10,11]. In this chapter, we investigated the electronics properties of both II-VI ternary alloys ($ZnO_{0.5}S_{0.5}$, $ZnO_{0.5}S_{0.5}$) and O doped in ZnS ($Zn_{16}O_1S_{15}$). For II-VI ternary alloys, GGA were used as exchange correlation energy to observe the electronic structure, PDOS and electron densities difference of the stable structure in Chapter 3 under high-pressure conditions. The electronic structures of O doped ZnS were revealed more precisely by HSE06 functional and also comparing with the GGA, to examine the PDOS of the stable structure under high-pressure. The information about these results are vital for band gap engineering in this type of materials.

4.1 The electronic structure of $ZnO_{0.5}S_{0.5}$ and $ZnO_{0.5}S_{0.5}$

The Chalcopyrite's electronic structure of both $ZnO_{0.5}S_{0.5}$ and $ZnO_{0.5}Se_{0.5}$ at 0 GPa condition were shown in Fig. 23 and 24 respectively. According to Fig. 23 and 24, both of Chalcopyrite $ZnO_{0.5}S_{0.5}$ and $ZnO_{0.5}Se_{0.5}$ are direct band gap semiconductors at gamma point. Their corresponding energy gaps at 0 GPa are 1.193 and 0.675 eV respectively. Additionally, more calculation results of energy gaps of Chalcopyrite $ZnO_{0.5}S_{0.5}$ and $ZnO_{0.5}Se_{0.5}$ at various pressures and those from others works are listed in table 7.

Furthermore, we investigated the atomic state characters of the electron Bloch wave function in both valence and conduction band at ambient and 30 GPa pressures by computing the total density of state (DOS) and partial density of state (PDOS) of both $ZnO_{0.5}S_{0.5}$ and $ZnO_{0.5}Se_{0.5}$. The results are shown in Fig. 25 From Fig. 25a, DOS

and PDOS of $ZnO_{0.5}S_{0.5}$ show that, in the case of $ZnO_{0.5}S_{0.5}$, the top of valence band (VB) is occupied by S-3p and p-d hybridization (Zn-3d, Zn-4p, S-3p, and O-2p) while the conduction band (CB) is dominated by Zn-pd hybridization. At the 30 GPa (Fig. 25b), the bottom of CB, slightly shifts away above the Fermi level corresponding to wider band gap at higher pressure. Moreover, applying pressure causes the VB broadening and S-3p PDOS lowering at around -1 eV below the Fermi level (see Fig. 25a and b). For $ZnO_{0.5}Se_{0.5}$ as the case, The DOS and PDOS near the band edge are almost the same as $ZnO_{0.5}S_{0.5}$ is the case. The difference is just it is Se-4p instead of S-3p (see Fig. 26).

Also, we analyzed the electron density difference of both Chalcopyrite alloys at 0 GPa as shown in Fig. 27 It indicates that bonding between Zn-O and Zn-S (Se) have ionic characters. The blue zone near the Zn cation indicates that the electrons transfer from Zn cation to those O and S (Se) anion. Electron densities slightly increase near O than S (Se) comparing with isolated O and S atoms due to the higher electronegativity of O than S (Se) atoms. Additionally, at high pressure up to 30 GPa, we found that nature of bonding between Zn, O, and S (Se) are still ionic.

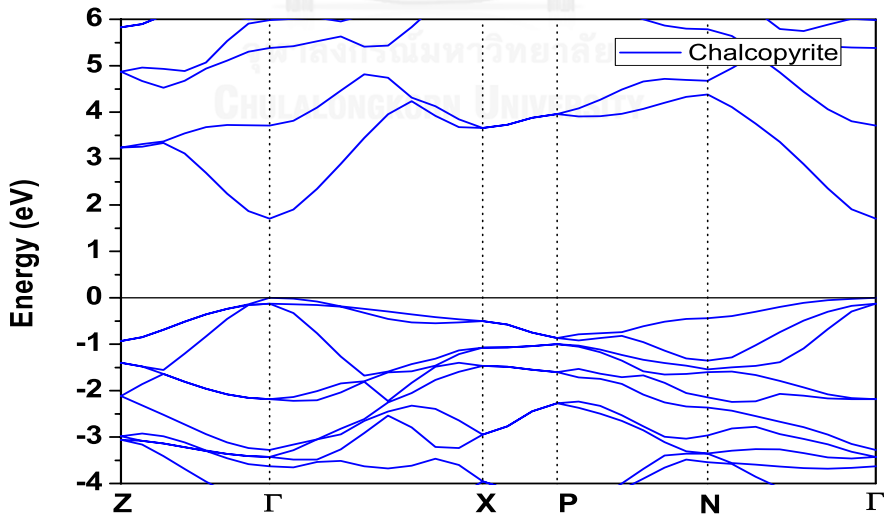

Figure 23: The electronic band structure of $ZnO_{0.5}S_{0.5}$Chalcopyrite structures at 0 GPa.

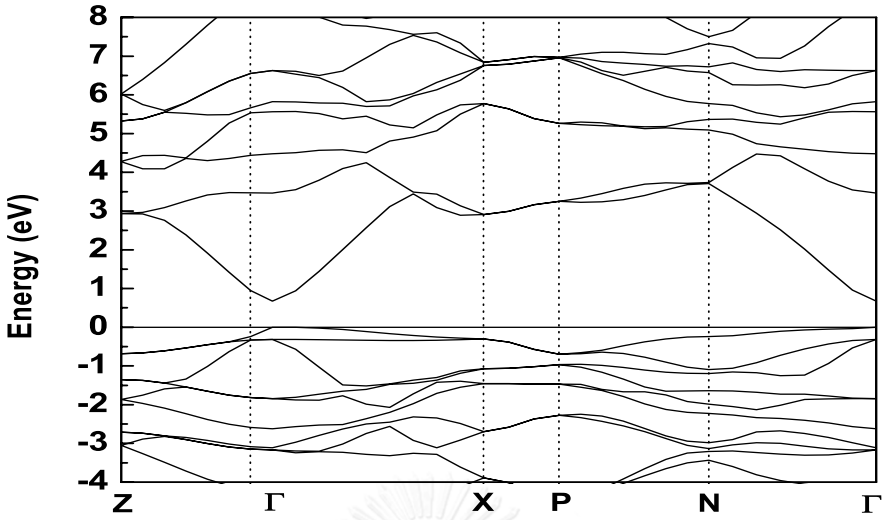

Figure 24: The electronic band structure of $ZnO_{0.5}Se_{0.5}$Chalcopyrite structures at 0 GPa.

Table 7: The energy gap of $ZnO_{0.5}S_{0.5}$ and $ZnO_{0.5}Se_{0.5}$ with various pressures.

Pressure (GPa)	$ZnO_{0.5}S_{0.5}$ Band gap (eV)	$ZnO_{0.5}Se_{0.5}$ Band gap (eV)
0	1.193,2.83[9], 1.44[6], 1.39[8]	0.675, 0.694[8]
10	1.475	0.998
20	1.703	1.255
30	1.924	1.484

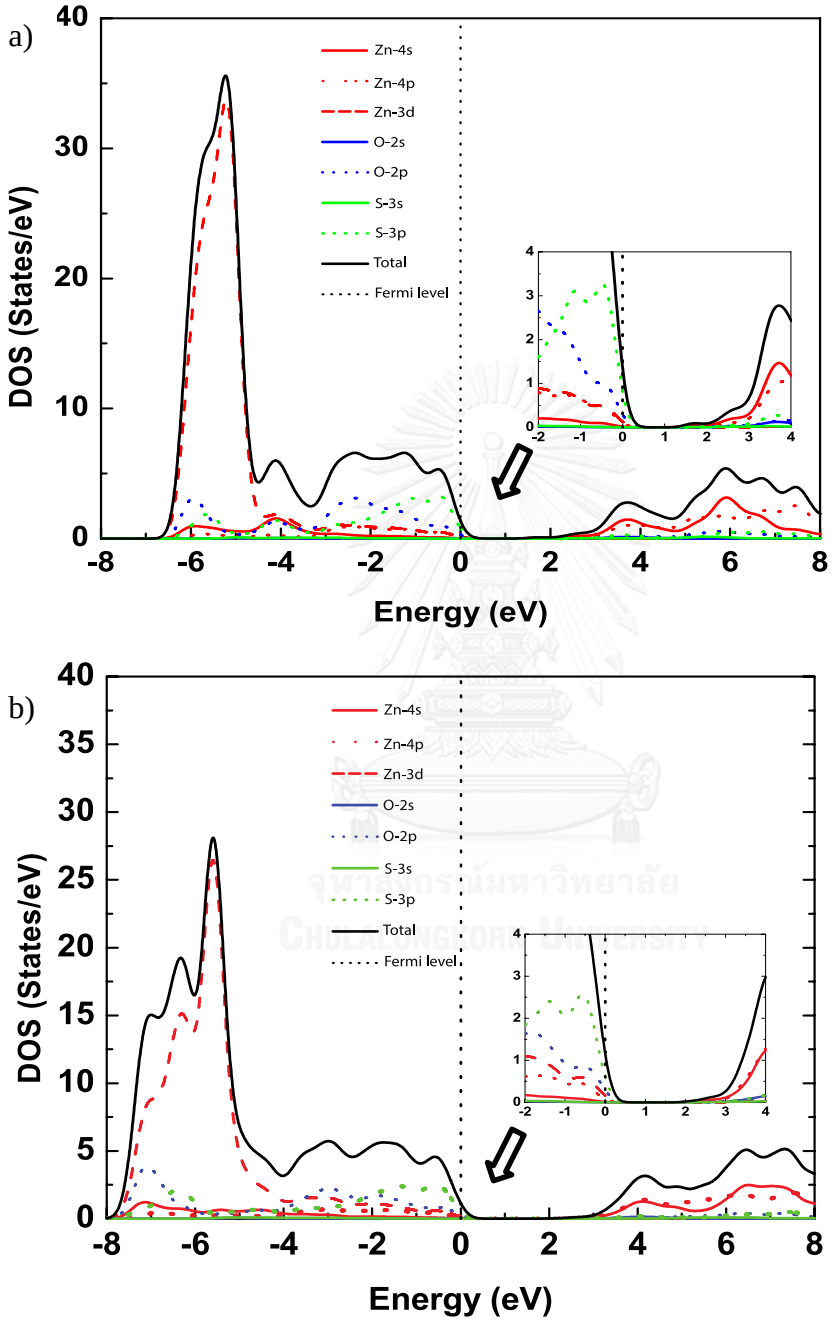

Figure 25: The PDOS of chalcopyrite structure of $ZnO_{0.5}S_{0.5}$ at a) 0 GPa and b) 30 GPa. The color representations of atomic orbitals are as following fashion: red for the Zn atomic orbital, blue for the O atomic orbital, yellow for S atomic orbital, and orange for Se atomic orbital. The s orbitals are represented by solid line, p by dotted line, d by dashed line, and total DOS by dark black dashed line. The PDOS near the top of valence band states were magnified by figure inset.

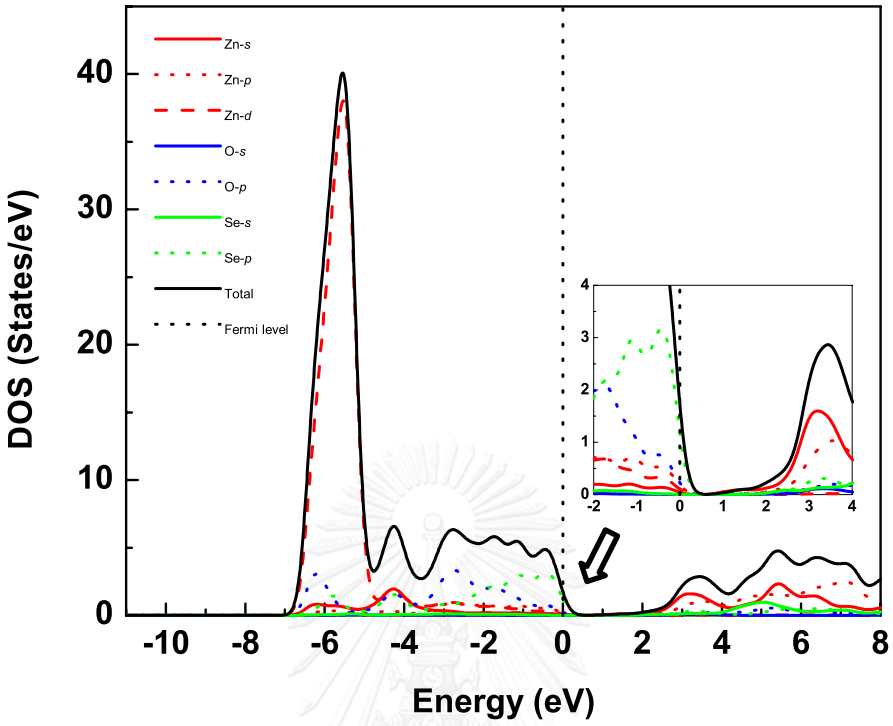

Figure 26: The PDOS of chalcopyrite structure of $ZnO_{0.5}Se_{0.5}$ at 0 GPa.

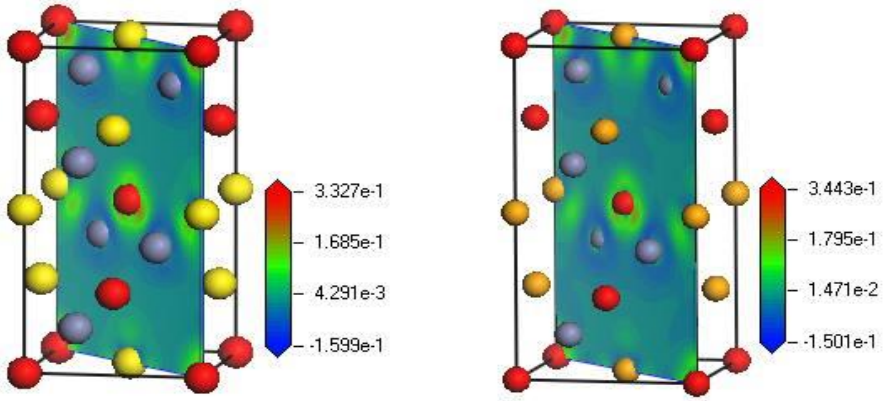

Figure 27: The electron densities difference of Chalcopyrite structure a) $ZnO_{0.5}S_{0.5}$ b) $ZnO_{0.5}Se_{0.5}$ at 0 GPa.

4.2 The electronic structure of $Zn_{16}O_1S_{15}$

As mention in the previous chapter, both Zincblende and Wurtzite structures occurred during the films preparation with difference conditions. We calculated the electronic structures of $Zn_{16}O_1S_{15}$ system at ambient and also high-pressure conditions, from 0 to 20 GPa, using HSE06 and GGA exchange correlation functionals. The results are shown in Fig. 28 and 29 for Zincblende and Wurtzite respectively. As seen in Fig. 28 and 29, Zincblende and Wurtzite structures are direct band gap semiconductors at Gamma point with deep O-3s state located in the fundamental band gap of ZnS. This is the local state as described by Ishikawa and Nakayama [14] that causes $Zn_{16}O_1S_{15}$ becoming a multiple band gap semiconductor defined by E_1 and E_2 in Fig. 28. E_1 and E_2 respectively represent a primary and secondary band gaps. At ambient pressure, HSE06 and GGA functionals yield the same trend in electronic structures at the band edges and at the middle of the gap. Table 8 lists all calculated pressure dependent energy gaps. To elucidate effects of pressure on the energy gaps, we calculate HSE06 pressure-dependent energy gaps of both structures at a number of pressures. Interestingly, E_1 increases while E_2 decreases with increasing in pressure for Zincblende structure. For Wurtzite structure, E_1 and E_2 increase as pressure increase with faster rate of E_2 in the low pressure range, $P \leq 10$ GPa, and faster rate of E_1 in the high pressure range, $P \geq 10$ GPa. This can be easily seen from the change of ΔE. Our results provide basic knowledge and enable the flexibility of band gap engineering in this class of material by varying pressure. Additionally, this knowledge on pressure–dependent of optical band gap may provide an alternative way for structure characterization by observing its optical transition as a function of pressure.

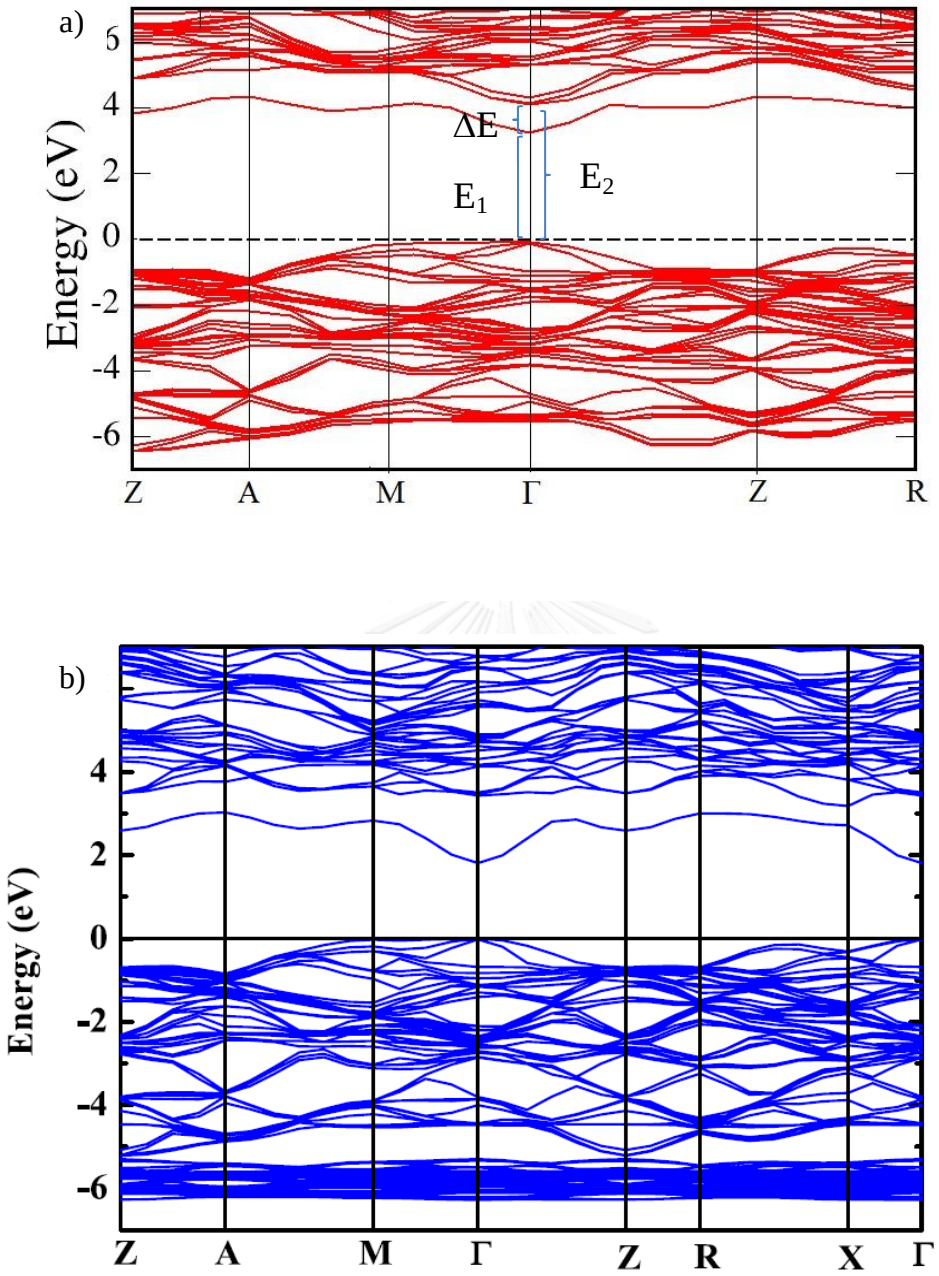

Figure 28: The electronic band structure at 0 GPa of $Zn_{16}O_1S_{15}$ in Zincblende structure using a) HSE06 b) GGA. The primery band gap (E_1), secondary (E_2) and their difference (ΔE) were shown.

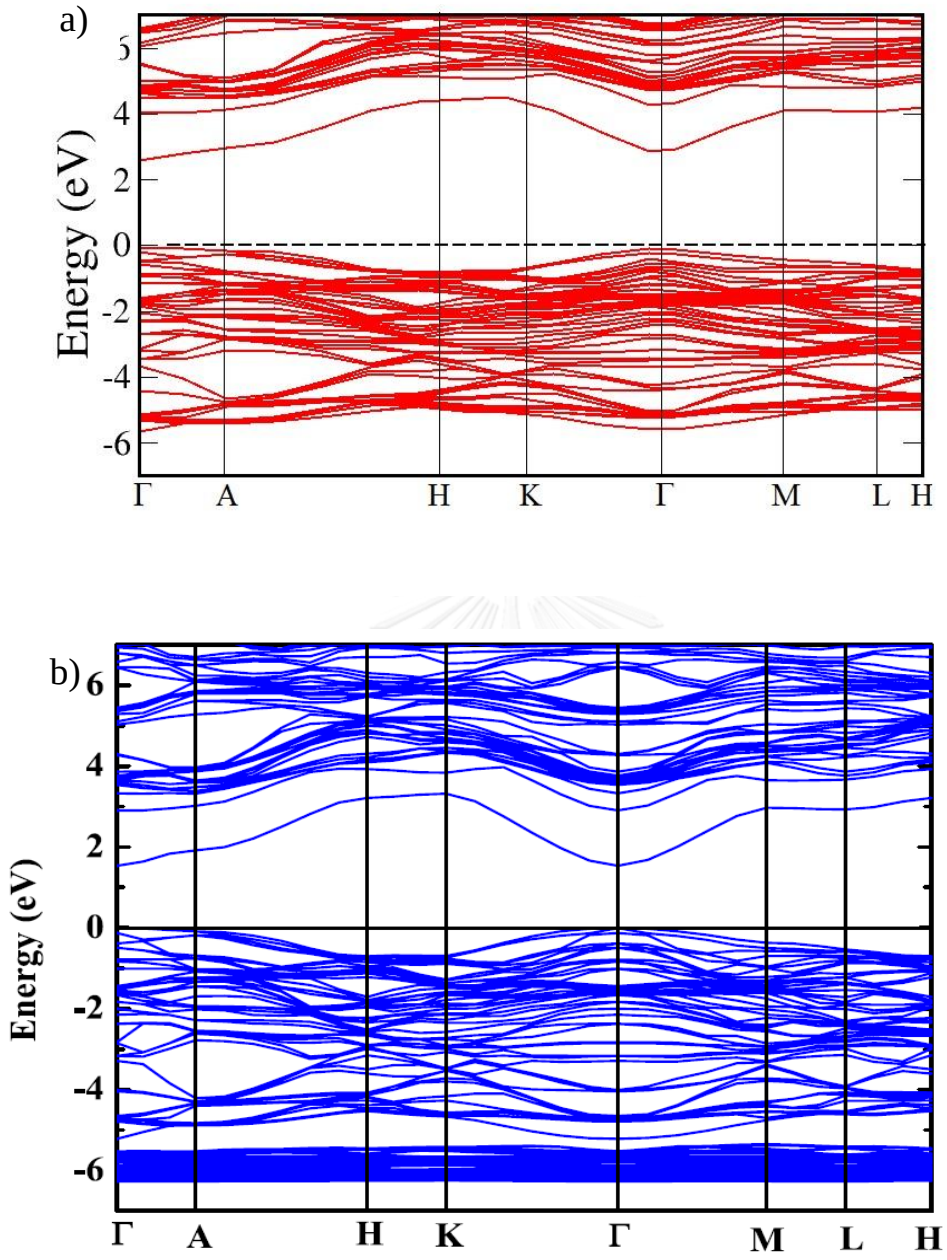

Figure 29: The electronic band structure at 0 GPa of $Zn_{16}O_1S_{15}$ in Wurtzite structure using a) HSE06 b) GGA..

Table 8: The primary, secondary and their different energy gap of $Zn_{16}O_1S_{15}$ in Zincblende and Wurtzite structure with various pressures.

Zincblende				**Wurtzite**		
Pressure (GPa)	E_1 (eV)	ΔE (eV)	E_2 (eV)	E_1 (eV)	ΔE (eV)	E_2 (eV)
0	2.94	1.48	4.42	2.61	1.39	4.00
10	3.31	0.87	4.18	2.79	1.51	4.30
20	3.46	0.53	3.99	2.92	1.49	4.41

Due to the time consuming problem of electronic properties calculation by HSE06, so, we further qualitatively analyze the electronic states in both structures by performing total density of state (DOS) and partial density of state (PDOS) calculations. According to Fig. 30, for both structures, DOS and PDOS illustrate that the top of valence band (VB) is mainly occupied by S-3p with small contribution of Zn-4s and p-d hybridyzation (Zn-4p, Zn-3d, and O-2p). While the bottom of conduction band is dominated by Zn-s and 4p orbital with S-s and doped O-3s state. These are surprising results compared with Ishikawa *et al.* [14] in which electronic structures of Zincblende $Zn_{32}O_1S_{31}$ and $Zn_{32}O_1Se_{31}$ were obtained by performing density functional based calculations allowing GGA-PBE96 as exchange–correlation functional. In this work, there exists no O-3s state in-between VB and CB. On the other hand, the hybridization state between O-3s and host ZnS locates in CB [14]. In contrast, our results reveal that the O-induced state exist in both Zincblende and Wurtzite structures. The DOS and PDOS of Wurtzite and those of Zincblende are fairely the same in shape but with the larger gap for the former [see Fig. 30]. Moreover, the density of intermediate O-3s state of Zincblende structure is higher than that of Wurtzite which correspond to higher optical transition rate of electrons from VB into the intermediate state and from the intermediate state into host CB.

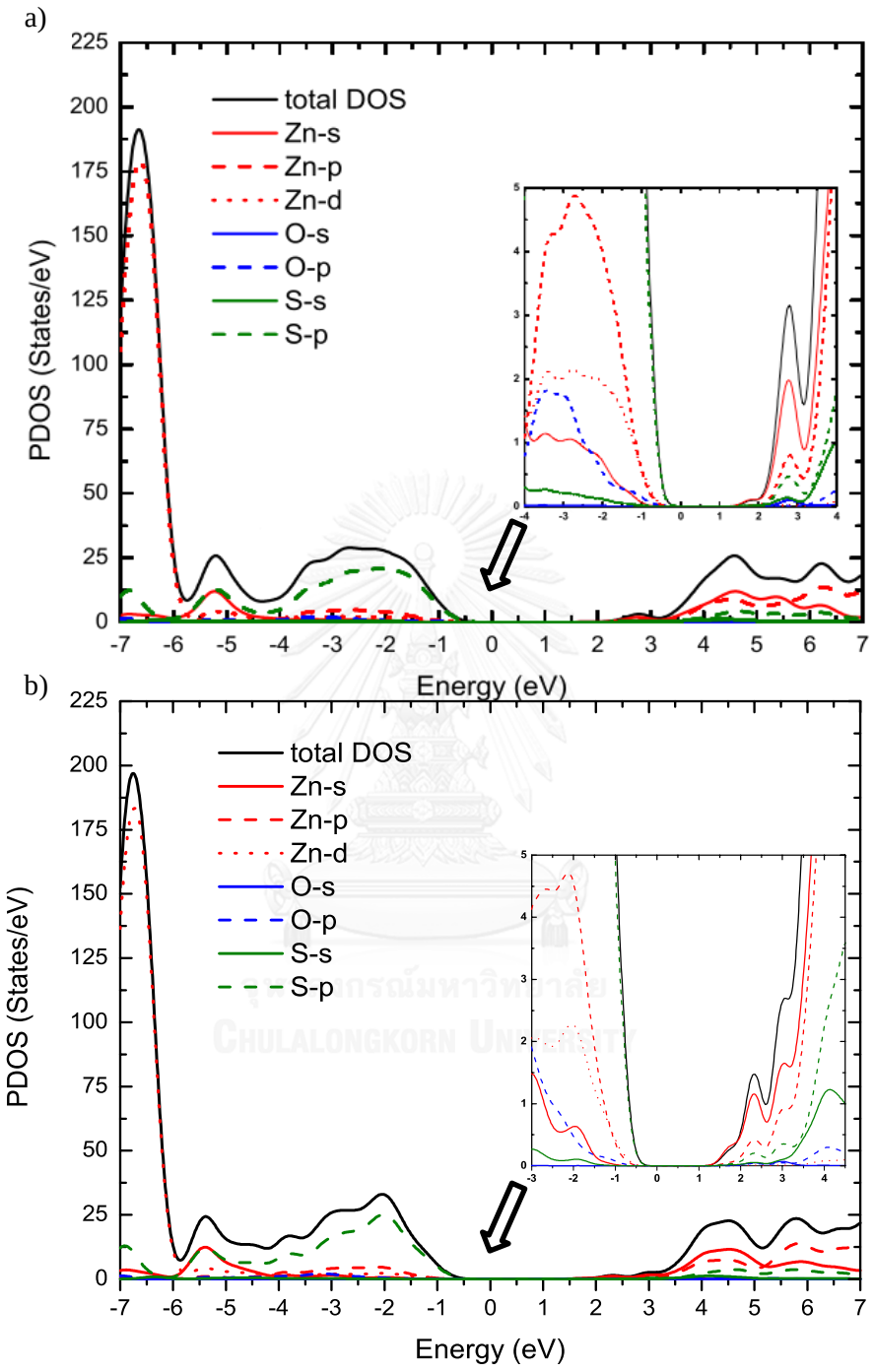

Figure 30: The PDOS of $Zn_{16}O_1S_{15}$ at 0 GPa of a) Zincblende and b) Wurtzite. The color representations of atomic orbitals are as following fashion: red for the Zn atomic orbital, blue for the O atomic orbital and green for S atomic orbital. The s orbitals are represented by solid line, p by dash line, d by dotted line, and total DOS by dark black dashed line. The PDOS near the top of valence band states were magnified by figure inset.

Chapter 5
Conclusion

Structural stability of five phases of $ZnO_{0.5}S_{0.5}$ and $ZnO_{0.5}Se_{0.5}$ have been examined at ambient pressure and high pressure up to 30 GPa within the GGA approximation density functional theory. The total enthalpy, Phonon dispersions, Born criteria and MD calculations have been used for structural stability verification at both ambient and high pressure conditions. From our results, it turns out that Chalcopyrite is a stable structure up to 10 GPa for both alloys. On the other hand, even though the CuAu-I has the lowest enthalpy at 27 and 30 GPa for $ZnO_{0.5}S_{0.5}$ and $ZnO_{0.5}Se_{0.5}$ respectively, it does not satisfy the Born criteria. Moreover, their 30 GPa and room temperature MD results do not converged within 5 ps simulation time and there is no sign for convergence from our calculation. This imply that the CuAu-I structure is unstable under those conditions. Also, in this work, we report the equilibrium lattice parameters, bulk modulus under ambient pressure and electronic structures at both ambient and high pressures. The electronic structures show that they are direct band gap at gamma point semiconductors and their energy band gaps vary in the same fashion with the increasing pressure, the higher pressure the wider band gap. For both alloys, the PDOS analysis shows that, up to 10 GPa, applying pressure does not change the atomic state characters of electronic states near the top of valence and the bottom of conduction bands, but mainly modifies the dominated Zn-3d atomic state of the deep Bloch state at -1 eV below Fermi level.

For $Zn_{16}O_1S_{15}$, two candidate structure namely Zincblende and Wurtzite structures have been investigated at ambient and high pressure up to 20 GPa using the GGA as exchange correlation functional. In order to obtain more accurate energy gap, the HSE06 hybrid functional were used comparing with GGA. The total enthalpy, Phonon dispersions and Born criteria have been used for structural stability verification at both ambient and high pressure conditions. The results yield that Zincblende structure is the lowest enthalpy at 0 GPa and phase transition between Zincblende to Wurtzite occurred around ~42 GPa. This result is alternative path of pure ZnS [12]. At 0 GPa condition, the enthalpy difference between Zincblende and

Wurtzite was only 0.238 eV. Thus, both structures can be prepared in energetically point of view. For Zincblende structure, The phonon dispersion and elastic constants show that this structure is mechanical stable at 0 to 10 GPa and unstable at 20 GPa as the former reaches negative values and the latter violate the Born criteria. In contrast, the Wurzite structure obeys both mechanical stability conditions at a range of pressure from 0 to 20 GPa. For electronic properties, both Zincblende and Wurtzite structures are direct band gap semiconductors at Gamma point with deep O-3s state located in the fundamental band gap of ZnS. This is the local state as described by Yu *et al.* [13] that causes $Zn_{16}O_1S_{15}$ becoming a multiple band gap semiconductor defined by the direct energy gaps. DOS and PDOS illustrate that the top of valence band (VB) is mainly occupied by S-3p with small contribution of Zn-4s and p-d hybridyzation (Zn-4p, Zn-3d, and O-2p). While the bottom of conduction band is dominated by Zn-s and 4p orbital with S-s and doped O-3s state. This knowledge on pressure – dependent of optical band gap may provide an alternative way for structure characterization by observing its optical transition as a function of pressure which leads to band gap engineering in optoelectronic device.

REFERENCES

1. Shan, W., et al., *Band Anticrossing in GaInNAs Alloys.* Physical Review Letters, 1999. **82**(6): p. 1221-1224.
2. Wu, J., et al., *Effect of band anticrossing on the optical transitions in $GaA_{1-x}N_x$/GaAs multiple quantum wells.* Physical Review B, 2001. **64**(8): p. 085320.
3. Wei, S.-H. and A. Zunger, *Giant and Composition-Dependent Optical Bowing Coefficient in GaAsN Alloys.* Physical Review Letters, 1996. **76**(4): p. 664-667.
4. Lehr, D., et al., *Band-Gap Engineering of Zinc Oxide Colloids via Lattice Substitution with Sulfur Leading to Materials with Advanced Properties for Optical Applications Like Full Inorganic UV Protection.* Chemistry of Materials, 2012. **24**(10): p. 1771-1778.
5. Meyer, B.K., et al., *Structural properties and bandgap bowing of $ZnO_{1-x}S_x$ thin films deposited by reactive sputtering.* Applied Physics Letters, 2004. **85**(21): p. 4929.
6. Rozale, H., et al., *A theoretical investigation of ZnO_xS_{1-x} alloy band structure.* physica status solidi (b), 2007. **244**(5): p. 1560-1566.
7. Fan, X.F., et al., *A theoretical study of thermal stability and electronic properties of wurtzite and zincblende ZnO_xS_{1-x}.* New Journal of Physics, 2009. **11**(9): p. 093008.
8. Thangavel, R., M. Rajagopalan, and J. Kumar, *First-principle calculations of structural stability of II-$O_{1-x}VI_x$ (II-Zn, Cd and VI-S, Se, Te) ordered chalcopyrite semiconductors.* Physica B: Condensed Matter, 2008. **403**(10-11): p. 1824-1830.
9. Khan, I. and I. Ahmad, *Theoretical studies of the band structure and optoelectronic properties of ZnO_xS_{1-x}.* International Journal of Quantum Chemistry, 2013. **113**(9): p. 1285-1292.
10. Pan, H.L., et al., *Characterization and properties of $ZnO_{1-x}S_x$ alloy films fabricated by radio-frequency magnetron sputtering.* Applied Surface Science, 2010. **256**(14): p. 4621-4625.
11. He, Y., et al., *Solubility limits and phase structures in epitaxial ZnOS alloy films grown by pulsed laser deposition.* Journal of Alloys and Compounds, 2012. **534**: p. 81-85.
12. Bilge, M., et al., *B3–B1 phase transition and pressure dependence of elastic properties of ZnS.* Materials Chemistry and Physics, 2008. **111**(2): p. 559-564.
13. Yu, K.M., et al., *Diluted II-VI oxide semiconductors with multiple band gaps.* Phys Rev Lett, 2003. **91**(24): p. 246403.
14. Ishikawa, M. and T. Nakayama, *First-principles study of oxygen-doping states in II-VI semiconductors.* physica status solidi (c), 2013. **10**(11): p. 1385-1388.
15. Herring, C., *A New Method for Calculating Wave Functions in Crystals.* Physical Review, 1940. **57**(12): p. 1169-1177.
16. Phillips, J.C. and L. Kleinman, *New Method for Calculating Wave Functions in Crystals and Molecules.* Physical Review, 1959. **116**(2): p. 287-294.
17. Hamann, D.R., M. Schlüter, and C. Chiang, *Norm-Conserving Pseudopotentials.* Physical Review Letters, 1979. **43**(20): p. 1494-1497.

18. Vanderbilt, D., *Soft self-consistent pseudopotentials in a generalized eigenvalue formalism.* Physical Review B, 1990. **41**(11): p. 7892-7895.
19. Mouhat, F. and F.-X. Coudert, *Necessary and sufficient elastic stability conditions in various crystal systems.* Physical Review B, 2014. **90**(22): p. 224104.
20. Grimvall, G., et al., *Lattice instabilities in metallic elements.* Reviews of Modern Physics, 2012. **84**(2): p. 945-986.
21. Payne, M.C., et al., *Iterative minimization techniques forab initiototal-energy calculations: molecular dynamics and conjugate gradients.* Reviews of Modern Physics, 1992. **64**(4): p. 1045-1097.
22. Segall, M.D., et al., *First-principles simulation: ideas, illustrations and the CASTEP code.* Journal of Physics: Condensed Matter, 2002. **14**(11): p. 2717.
23. Ashrafi, A. and C. Jagadish, *Review of zincblende ZnO: Stability of metastable ZnO phases.* Journal of Applied Physics, 2007. **102**(7): p. 071101.
24. Khenata, R., et al., *Elastic, electronic and optical properties of ZnS, ZnSe and ZnTe under pressure.* Computational Materials Science, 2006. **38**(1): p. 29-38.
25. Klingshirn, C.F., et al., *Zinc Oxide: From Fundamental Properties Towards Novel Applications*. 2010: Springer Berlin Heidelberg.
26. Andersen, H.C., *Molecular dynamics simulations at constant pressure and/or temperature.* The Journal of Chemical Physics, 1980. **72**(4): p. 2384.
27. Shay, J.L. and J.H. Wernick, *CHAPTER 1 - INTRODUCTION*, in *Ternary Chalcopyrite Semiconductors: Growth, Electronic Properties, and Applications*. 1975, Pergamon. p. 1-2.

APPENDIX

VITA

My name is Rut Manotum, a guy from southern of Thailand. I studied at Theppramit-suksa elementary school, Theppramit-suksa primary school and Suratthani high school near my home town. I graduated in B.Sc. at Prince of Songkla University, 2005 and M.Sc. at Chulalongkorn University, 2009.